Thesis for the Degree of Licentiate of Engineering

Study of Mutual Coupling in Finite Antenna Arrays for Massive MIMO Applications

Tomislav Marinović

CHALMERS

Department of Electrical Engineering
Antenna Systems
Chalmers University of Technology

Göteborg, Sweden 2020

Study of Mutual Coupling in Finite Antenna Arrays for Massive MIMO Applications

Tomislav Marinović

Department of Electrical Engineering
Antenna Systems
Chalmers University of Technology
SE–412 96 Göteborg
Sweden
Telephone: +46 (0)31–772 10 00
Email: tommar@chalmers.se

Typeset by the author using LaTeX.

Chalmers Reproservice
Göteborg, Sweden 2020

To my family

Abstract

This thesis focuses on the study of mutual coupling (MC) in finite antenna arrays for base station antennas (BSAs) for Massive multiple-input multiple-output (MIMO) applications, with an emphasis on the development of a computationally-efficient modeling technique for the analysis of MC which can be readily applied in the design or synthesis schemes for BSAs. Traditionally, the effects of MC have been ignored or underestimated in the analyses performed within the information-theoretic-based communities by assuming idealized antenna elements with no MC between them or by considering the fictitious isotropic radiator models. In contrast, this thesis demonstrates the essentialness of proper modeling and inclusion of the physical antenna effects in the models used to predict the performance of a Massive MIMO system, as evidenced through the performed sum-rate analysis of a downlink line-of-sight (LoS) MIMO system in the presence of MC.

The developed model for the analysis of MC is inspired by the concept of multiple scattering by which the overall effect of the antenna array MC can be determined by cascading the scattering responses of all array elements. Such an approach requires the full-wave characterization of only a single element in isolation, while the mutual interactions between different elements are modeled by approximating the incident field as a single plane wave with mutually-orthogonal polarization taken from the spherical wave expansion (SWE) of the field scattered from any other array element. This process is described mathematically through the iterative scheme based on the classical Jacobi and Gauss-Seidel iterative methods.

Additionally, a sum-rate model of a downlink LoS multi-user MIMO system including the MC, has been developed. Herein, the effects of MC are accounted through the S-matrix of the BSA and the embedded element patterns (EEPs) of all BSA elements, which are used to approximate the channel matrix in a LoS environment. The S-matrix and the EEPs obtained by using the Jacobi-based MC model have been incorporated into the MIMO system model, showing good agreement in terms of the achievable sum rate compared to the reference result which uses the MoM-based simulation data. The accuracy and run-time benefits of the Jacobi-based model make it a possibly promising candidate for use in BSA design and synthesis applications, particularly when large array configurations need to be (repeatedly) analyzed.

Keywords: 5G, base station antenna (BSA), Massive MIMO, mutual coupling (MC), multiple scattering, iterative methods.

Preface

This thesis is in partial fulfillment for the degree of Licentiate of Engineering at the Chalmers University of Technology, Göteborg, Sweden.

The work resulting in this thesis was carried out between December 2016 and June 2020 at the TELEMIC Division, Department of Electrical Engineering (ESAT), KU Leuven, Leuven, Belgium and Antenna Systems Unit, Department of Electrical Engineering, Chalmers University of Technology, Göteborg, Sweden. The doctoral program involved the industrial secondments at TNO, The Hague, and NXP, Eindhoven, both the Netherlands, and Ericsson AB, Göteborg, Sweden - in total duration of 21 months. Professor Guy A. E. Vandenbosch of KU Leuven is the main supervisor. In addition, Associate Professor Rob Maaskant of the Chalmers University of Technology is the co-supervisor and examiner.

This project has received funding from the European Union's Horizon 2020 research and innovation program under the Marie Skłodowska-Curie grant agreement No. 721732.

Acknowledgment

During the past years as a PhD student, I have had the privilege to enjoy the company of many special people. First and foremost, I would like to express my deepest gratitude and admiration to my mentors - Prof. Guy Vandenbosch (KU Leuven) and Prof. Rob Maaskant (Chalmers University of Technology), for providing me with this opportunity, for their trust, guidance, support and patience, and for instilling the priceless lessons which extend beyond the realms of science. I have benefited tremendously from their leadership, passion, vision, ethics, wisdom and technical insight, both professionally and personally.

Furthermore, I would like to acknowledge all the SILIKA members, both the project management and fellow PhD candidates, who have helped to create a unique and thriving working environment. Particularly, I wish to express my gratitude to Martin Johansson and Anders Stjernman (Ericsson AB), Dave Bekers (TNO) and Anton de Graauw (NXP) for welcoming me to their institutions, for their time and valuable advice and contributions. To Martin, I will always be thankful for your support, and I have learned a lot from your model-professional and practical approach and your problem-solving and coding skills. To Anders, I have enjoyed your illuminating insights into the nature and aspects of mutual coupling, and our vivid discussions onto this topic. To Dave, I am grateful for your contributions with regards to the paper structure and writing, and for setting an example on the principles of scientific thinking, writing and attention to detail. Similarly, I wish to thank Prof. Dirk de Villiers for his vision of the paper development and for having welcomed me at the Stellenbosch University during my visit in April 2019.

Also, I wish to acknowledge the supporting staff at different institutions I have been a part of, for their kindness, help and availability. Particularly, I would like to thank Natalie Buyckx (KU Leuven) for providing a timely and impeccable assistance and valuable information during this period. Additionally, I wish to thank Graziella del Savio (KU Leuven), Prof. Marianna Ivashina, Prof. Christian Fager and Jens Hansson (all Chalmers) for their efforts on initiating the doctoral double-degree agreement between KU Leuven and Chalmers University of Technology. Without their perseverance, the agreement, and consequently this thesis, would not be attainable.

Moreover, I wish to thank Prof. Raj Mittra for accepting the role of the discussion leader at the upcoming thesis defense.

Additionally, I would like to send my warmest regards to my dear friends in Leuven - Tomislav, Mario, Ivan, Adrián, Eduardo and Marzieh, for their continuous support, understanding and all the pleasant moments and lasting memories that we have shaped together.

Finally, I dedicate this thesis to my family for their love and encouragement throughout this period.

List of Publications

This thesis is based on the work contained in the following appended papers:

Paper A
T. Marinović, D. I. L. de Villiers, D. J. Bekers, M. N. Johansson, A. Stjernman, R. Maaskant and G. A. E. Vandenbosch, "Fast Characterization of Mutually-Coupled Array Antennas Using Isolated Antenna Far-Field Data," *IEEE Transactions on Antennas and Propagation*, vol. 68, no. (unassigned), 2020 (in press).

Paper B
T. Marinovic, A. Farsaei, R. Maaskant, A. Lahuerta-Lavieja, M. N. Johansson, U. Gustavsson and G. A. E. Vandenbosch, "Effect of Antenna Array Element Separation on Capacity of MIMO Systems Including Mutual Coupling," in *Proceedings of the 2019 IEEE International Symposium on Antennas and Propagation and USNC-URSI Radio Science Meeting (AP-S/URSI)*, Atlanta, GA, USA, 7-12 Jul. 2019.

Other related publications of the Author not included in this thesis:

- J. Zhang, S. Yan, X. Hu, T. Marinovic and G. A. E. Vandenbosch, "A Multi-Functional Compact Button Antenna for Wearable Applications," in *Proceedings of the 14th European Conference on Antennas and Propagation (EuCAP)*, Copenhagen, Denmark, 15-20 Mar. 2020.

- M. Kupresak, T. Marinovic, X. Zheng, G. A. E. Vandenbosch and V. V. Moshchalkov, "Nonlocal Hydrodynamic Response of Plasmonic Structures at Deep-nanometer Scale," in *Proceedings of the 62nd International Symposium ELMAR-2020*, Zadar, Croatia, 14-15 Sep. 2020.

- M. Kupresak, T. Marinovic, X. Zheng, G. A. E. Vandenbosch and V. V. Moshchalkov, "Hydrodynamic Approach for Deep-nanometer Scale Topologies: Analysis of Metallic Shell," submitted to *International Symposium on Antennas and Propagation (ISAP 2020)*, Osaka, Japan, 25-28 Jan. 2021.

- T. Marinović, M. Kuprešak, R. Maaskant and G. A. E. Vandenbosch, "On the Convergence of the Iterative Gauss-Seidel-Based Electric Field Algorithm for the Solution of Antenna Array Mutual Coupling," submitted to *International Symposium on Antennas and Propagation (ISAP 2020)*, Osaka, Japan, 25-28 Jan. 2021.

Acronyms

5G	Fifth Generation
ACA	Adaptive Cross Approximation
ARC	Active Reflection Coefficient
AWGN	Additive White Gaussian noise
BS	Base Station
BSA	Base Station Antenna
CBFM	Characteristic Basis Function Method
CBFP	Characteristic Basis Function Pattern
CEM	Computational Electromagnetics
CMS	Canonical Minimum Scattering
CSI	Channel State Information
DDM	Domain-Decomposition Method
DGFM	Domain Green's Function Method
DL	Downlink
EE	Energy Efficiency
EEP	Embedded Element Pattern
ELAA	Extremely Large Aperture Array
EM	Electromagnetic
EWC	Expansion Wave Concept
FDTD	Finite-Difference Time-Domain
FEM	Finite-Element Method
FoV	Field-of-View
GSM	Generalized Scattering Matrix
IE	Integral Equation
IEP	Isolated Element Pattern
ISA	Irregular Sparse Array
LEGO	Linear Embedding via Green's Operators
LoS	Line-of-Sight

M2M	Machine-to-Machine
MBF	Macro Basis Function
MLFMM	Multilevel Fast Multipole Method
MoM	Method of Moments
(MU-)MIMO	(Multi-User-) Multiple-Input Multiple-Output
NLoS	Non-Line-of-Sight
PDE	Partial Differential Equation
PIFA	Planar Inverted-F Antenna
PWS	Plane-Wave Spectrum
SE	Spectral Efficiency
SFX	Synthetic Function
SNR	Signal-to-Noise Ratio
SWE	Spherical Wave Expansion
TDD	Time-Division Duplex
UE	User Equipment
UL	Uplink
ULA	Uniform Linear Array

Contents

Part I

Introductory Chapters

Chapter 1

Introduction

1.1 Towards Massive MIMO

The technological and socioeconomic dynamics of a modern society have become increasingly correlated with the evolution of mobile communication systems [1]. Each year, various new devices with enhanced capabilities are developed, altering the way people coordinate their daily routines and business practices. The projection of the annual growth of connected devices up to 2023 is illustrated in Fig. 1.1, showing an increased presence of machine-to-machine (M2M) connections [2], typically used in smart sensing and smart monitoring applications. Additionally, the quantitative increase in the number of connections is followed by the demand for high-quality service. Particularly, the growth potential of promising technologies such as virtual reality, augmented reality or tactile Internet is correlated with advances in terms of high-speed and low-latency connection [3–5]. Two conclusions can be drawn: first, the demand for throughput continuously increases and second, the amount of available spectrum is limited [6].

The solution to this challenge requires an innovating approach in the design and implementation of mobile communication systems - leading to the fifth-generation mobile communication systems (5G). The necessity of the evolution to next-generation mobile communication systems has been recognized by the European Commission and communicated through a document entitled "*5G for Europe: An Action Plan*" [7], and supported through the Horizon 2020 funding program. The potential use cases of 5G technology with regards to the throughput and latency requirements are listed in Fig. 1.2. The total amount of data (throughput) that can be communicated by a mobile network is given as [8]

$$\underbrace{\text{throughput}}_{[\text{bits/s/km}^2]} = \underbrace{\text{cell density}}_{[\text{cells/km}^2]} \times \underbrace{\text{available RF spectrum}}_{[\text{Hz}]} \times \underbrace{\text{spectral efficiency}}_{[\text{bits/s/Hz/cell}]}. \quad (1.1)$$

To fulfill the promise of increased data rates, an additional chunk of the unused

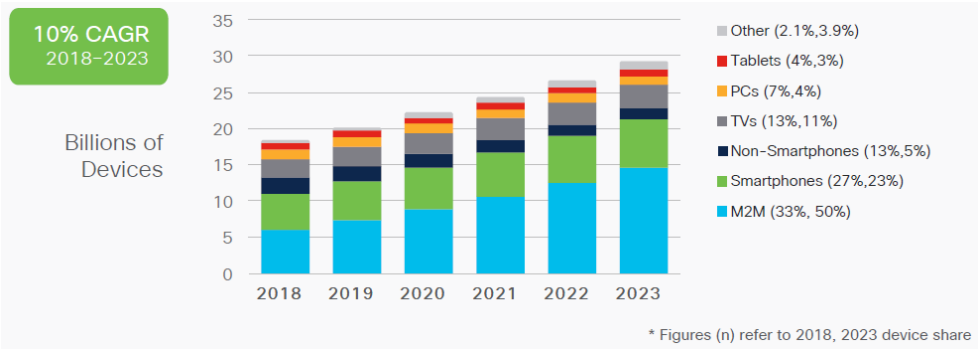

Figure 1.1: Annual growth projections of connected devices. CAGR denotes the *compound annual growth rate*. Source: Cisco [2].

mm-wave spectrum above 26 GHz (Ka band) has been allocated for 5G usage. However, electromagnetic (EM) waves propagating in the mm-wave range exhibit higher losses compared to the waves propagating in the long-wave (L) or short-wave (S) bands. Additionally, the output power of solid-state circuits in the mm-wave region is limited [9]. Consequently, coverage of a given area requires denser base stations deployment which in turn increases the complexity and thus the costs of the infrastructure. The throughput of a 5G system benefits from the increased amount of available spectrum, as suggested by Eq. (1.1). However, the throughput rewards in 5G are primarily due to greatly improved spectral efficiency (SE) by employing the Massive multiple-input multiple-output (MIMO) technology [10, 11].

1.2 Massive MIMO Technology

The idea of multi-user MIMO (MU-MIMO) in which a base station (BS) simultaneously serves multiple user equipments (UEs) has been present since the 80s [12–14]. Despite some trials, it has not become a commercial success in the 90s or 00s [15].

The concept of Massive MIMO, introduced by Marzetta in 2010 [16], is built upon the initial promise of MU-MIMO technology and envisioned as its large-scale and scalable exponent. Since then, it has instigated a wave of research and development activities in both the industry and the academia.

In the Massive MIMO system, the base station equipped with a large number of antennas communicates with multiple users using the same time-frequency resource, over a time-division duplex (TDD) channel. The channel vectors between the base station and UE terminals are assumed as nearly orthogonal, which enables the optimal performance of linear precoding algorithms including the ability of simultaneous transmission of multiple data streams on the downlink without inter-channel interference [17]. The assumption of near-perfect channel vector orthogonality is known as *favorable propagation* in the Massive MIMO literature [15, 17]. The channel state

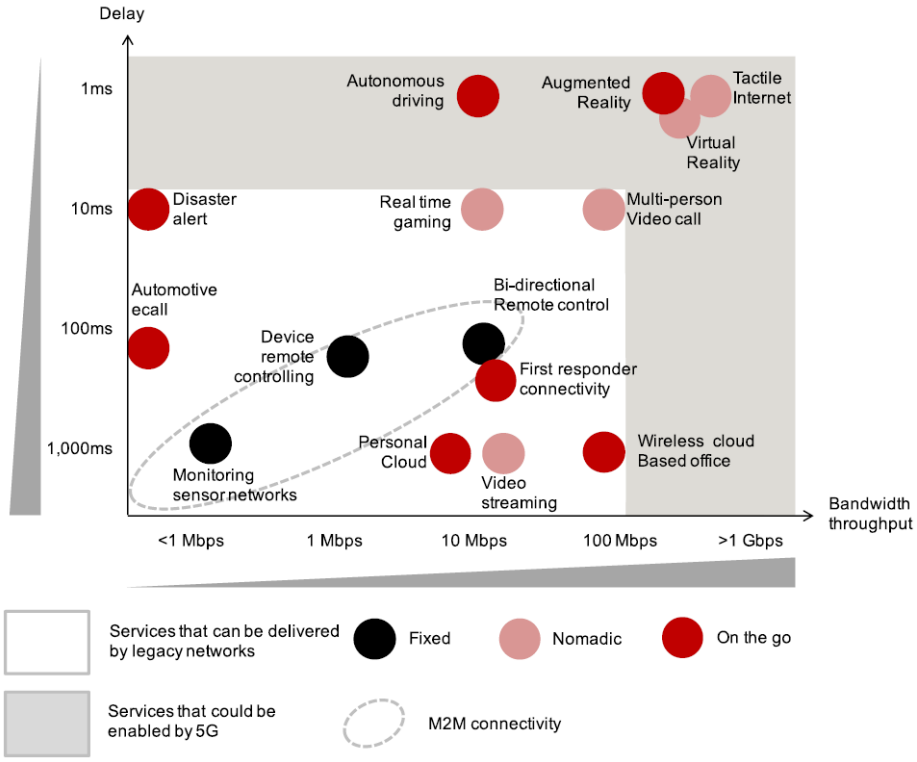

Figure 1.2: Throughput and latency (delay) requirements of potential 5G use cases. Source: GSMA Intelligence [4].

information (CSI), a fundamental system variable, is acquired (measured) at the BS by using the uplink pilot signals and exploiting the uplink-downlink channel reciprocity [18]. Linear signal processing [19], based on the acquired CSI, can be used at the BS in both the uplink and downlink modes to minimize the interference between the users, or constructively add different signal components at the receiver in a multipath propagation environment.

From the antenna-system perspective, the logic behind the Massive MIMO operation is relatively straightforward. Consider a BS with M antennas. The amount of power that can be transmitted by the base station antenna (BSA) is fixed by the RF chain specifications. The signal power received by a user is proportional to M, since a BSA with more elements can more efficiently focus the energy in the intended direction [15]. Consequently, with M antennas and assuming fixed radiated power, the received signal can be up to M times amplified [15]. In a system with K spatially-multiplexed users sharing the same time-frequency resource, the radiated power is shared between them, according to a specified power allocation scheme [15]. For simplicity, let us assume that each user is effectively allocated $1/K$ of the total power [15]. Then, if $M/K > 1$, the users will experience a stronger signal compared to a reference single-antenna BS setting (with identical power) [15]. In practice, M

needs to be much larger than K. By making M large, the Massive MIMO systems benefit in several ways. Firstly, large M is required to secure the asymptotic orthogonality between the users [6, 20]. Secondly, an increased array aperture due to the deployment of more antennas improves the spatial resolution of the BS, i.e., its ability to distinguish between different users [9]. Furthermore, large M allows the efficient suppression of interference. Finally, it can potentially reduce the required power for both the UL and DL operation [21], which is important from the ecological and economical [22], user-satisfaction (e.g., battery life) and health standpoints, the latter being particularly important amid increased public concerns regarding the safety of electromagnetic exposure [23, 24].

The scalability of Massive MIMO implies that, in theory, an infinite number of antennas can be utilized at the BS, serving a huge number of users. However, the system throughput improves only logarithmically with increasing M [6]. Additionally, the computational complexity of the CSI acquisition algorithms limits the number of users which can be simultaneously served by the BS, as noted in [6, 9, 25]. Finally, the number of antennas is limited by the available physical dimension, particularly in the spectrum below 6 GHz.

1.3 Antenna Systems for Massive MIMO Communications

The introduction of Massive MIMO brings forth a set of innovative strategies for the design and integration of large-scale antenna arrays.

1.3.1 Context and Design Strategy

The design of BSA arrays for Massive MIMO applications deviates from the classical textbook antenna design. It requires not only the understanding of applied electromagnetic theory, but also a global understanding of the functioning of a Massive MIMO system from the information-theoretic perspective. Moreover, in a multivariate system such as Massive MIMO, the initial array configuration might not yield a desired performance in terms of the spectral or energy efficiencies (EE) [11]. Hence, several design iterations might often be needed until the optimal array configuration can be found. The flowchart of such an iterative co-design strategy involving the electromagnetic and information-theoretic specifications is illustrated in Fig. 1.3. The analysis of mutual coupling (MC) in the BSA [26], in terms of the S-matrix $\boldsymbol{S}_{\mathrm{TT}} \in \mathbb{C}^{M\times M}$ and embedded element patterns (EEPs) of all elements, is required for the composition of the channel matrix, $\boldsymbol{H} \in \mathbb{C}^{K\times M}$. This data can be obtained through a measurement or a simulation. Similarly, the channel matrix requires the description of the S-matrix of the UEs. Assuming the single-antenna users with no MC between them, $\boldsymbol{S}_{\mathrm{RR}}$ is a diagonal matrix $\in \mathbb{C}^{K\times K}$. Additionally, the load impedances

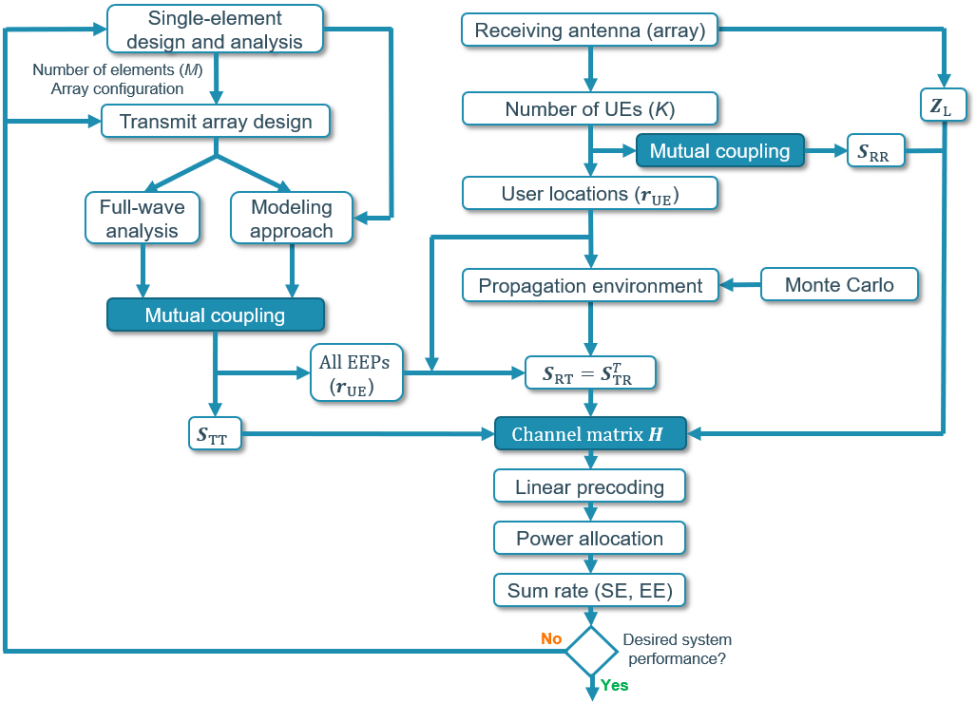

Figure 1.3: Electromagnetic and information-theory-based iterative co-design of a BSA for Massive MIMO applications (see also [9, Fig. 4.4]).

at the UEs' terminals may be modeled through a diagonal matrix $\boldsymbol{Z}_{\mathrm{L}} \in \mathbb{C}^{K\times K}$ [9]. Furthermore, the specifications of the propagation environment are embedded in the channel matrix through $\boldsymbol{S}_{\mathrm{RT}} = \boldsymbol{S}_{\mathrm{TR}}^{T} \in \mathbb{C}^{K\times M}$, which describes the electromagnetic interaction between the BSA and user terminals for the considered propagation scenario. Here, $\{\cdot\}^T$ denotes the transpose operator. In turn, the channel matrix determines the linear processing and power allocation at the BS, after which the system sum rate and consequently the spectral and energy efficiencies, can be estimated.

1.3.2 Research Directions for Antenna Arrays

In its beginnings [16], the Massive MIMO technology was confronted with skepticism, partly driven by negative past experience with the MU-MIMO [15]. Fast-forward a decade, the technology has evolved into a mature communication concept, evidenced by the existence of two textbooks [10, 11]. An excellent overview of the latest advances in Massive MIMO and the vision of future research has been given by Björnson *et al.* [15]. The authors envision five potential research directions for antenna arrays: 1) *Extremely large aperture array* (ELAA); 2) *Holographic Massive MIMO*; 3) *Six-dimensional positioning*; 4) *Large-scale MIMO radar* and 5) *Intelligent Massive MIMO*. While the latter three tend to focus on specific applications with their corresponding system specifications, the former two focus on the more general aspects

of antenna array deployment.

In the domain of ELAAs, some intriguing solutions have been proposed [15]. First, ELAAs are envisioned as conformal arrays mounted on an available surface, e.g., a side of a building, possibly with a relatively large antenna spacing in terms of wavelength. By increasing the array aperture, the spatial resolution of the BSA can be enhanced, thus increasing the odds of achieving favorable propagation conditions (near-perfect orthogonality between the channel vectors). Alternatively, ELAAs could potentially be realized using the *Cell-free Massive MIMO* concept [27], in which the single-antenna access points are distributed around the users and connected to a central processing unit. A possible shortcoming of using the ELAAs includes the increased likelihood of communicating through the near-field of a BSA due to its extremely large array aperture (and correspondingly large far-field distance), which complicates the channel modeling [15]. In contrast to ELAAs, the idea of a holographic Massive MIMO, inspired by the principles of optical holography, envisions a communication concept based on a spatially continuous aperture, which is formed by stacking a huge number of antennas into a fixed physical aperture [15]. A variety of potential use cases for the ELAAs and the holographic Massive MIMO are listed in Table I of the same reference.

Finally, the implementation of Massive MIMO involves two far-apart pieces of the spectrum — sub-6 GHz and mm-wave regions. Consequently, the hardware requirements and the channel characteristics might considerably differ. The challenges associated with the implementation of Massive MIMO in two distinct regions of the spectrum have been addressed in [28].

1.3.3 Sparse Arrays

Although the impact of antenna spacing in regular arrays for MU-MIMO communications has often been analyzed, a 0.5λ spacing has largely become the norm for practical system realizations, where λ denotes the wavelength. In Massive MIMO systems, that notion is being challenged, as outlined in [15]. Sparse arrays, which can be defined as arrays whose mean element spacing exceeds the conventional 0.5λ spacing [9], represent an interesting prospect for the deployment in Massive MIMO systems. Sparse arrays can be structured in the form of a lattice (periodic or aperiodic), or those that do not exhibit any discernible spatial patterning (irregular sparse arrays or ISAs).

So far, sparse arrays have been mainly deployed in satellite [29, 30] and radio-astronomy applications [31–33]. The use of sparse arrays in the context of Massive MIMO applications has been studied in [9]. Compared to conventional arrays with the half-wavelength closest spacing, the benefits of using the sparse arrays possibly include a reduced number of elements, reduced power variation and enhanced spatial resolution [9]. The main drawback of sparse arrays with a lattice in the context of

MIMO communication, is the appearance of grating (pseudo-grating) lobes. However, by using the ISAs, this limitation can be largely mitigated, as the grating lobes can be suppressed owing to the irregular array structure.

1.4 Aim of Research

The research has been performed within the "SILIKA" project funded by the European Union's Horizon 2020 program under the grant agreement No. 721732, aimed at developing innovating antenna systems for mm-wave 5G mobile communications. The direction of this individual research project has been partly driven by the requirements of SILIKA's work packages "*WP1 — Array architecture study and system-level comparison*" and "*WP3 —Design flow for co-design and integration of antennas and electronics*", and influenced by the doctoral double-degree agreement between KU Leuven and the Chalmers University of Technology, and the industrial secondments carried out at TNO, NXP and Ericsson.

The main research objective is the study of MC in (Massive) MU-MIMO systems. Mutual coupling represents an aggregate of all mutual interactions between the array elements, which alters the impedance and radiation pattern of an isolated element [34]. Accurate characterization of the coupling effects is important for both the element design and array design or synthesis. Additionally, the effect of MC may have a non-negligible impact on the performance of MU-MIMO systems, particularly when large array configurations need to be considered. Nevertheless, within the (Massive) MU-MIMO community, largely dominated by the information-theory-based research, the effect of MC is often underestimated or neglected, by assuming isolated or isotropic elements. However, strictly speaking, such approach is only valid when the ports are completely uncoupled, which rarely holds in practice [35, Ch. 3.3.1].

Therefore, a major research question concerns the estimation of MC in MU-MIMO systems and its impact on the overall system performance. The research goals addressed in this thesis can be summarized as follows:

- Analyzing the strategies for the analysis of antenna array MC, with a particular emphasis on the development of computationally-efficient MC models. This is particularly important in the context of iterative co-design of antenna arrays for Massive MIMO applications, where several large array configurations need to be rapidly analyzed, as illustrated in Fig. 1.3.

- Analyzing the impact of MC on the performance of (Massive) MU-MIMO systems, e.g., by analyzing the sum rate in the presence of MC.

- In the context of MC, searching for suitable elements and/or array configurations for the deployment in (Massive) MU-MIMO communication systems. Analyzing the use potential of sparse arrays.

1.5 Thesis Outline

This thesis is composed of two main parts. The first part, ordered in five chapters, summarizes the problem statement, research outcomes and the vision of future work. The second part contains the appended papers with a more detailed research description. Non-appended papers are listed in the section "List of Publications".

Regarding Part I, Chapter 1 motivates the research and places it within the context of emerging Massive MIMO communication systems. Chapter 2 details the impact of MC in (Massive) MU-MIMO systems and gives a brief overview of computational methods for the analysis of MC, thus providing a context for Chapter 3 where a novel computationally-efficient MC model is described. Chapter 4 introduces the sum-rate model of a downlink line-of-sight (LoS) MU-MIMO system in the presence of MC, which receives the input in terms of the MC from the model described in Chapter 3. Finally, Chapter 5 summarizes the thesis and provides guidelines for future research.

Part II appends the papers relevant for the discussion in Part I. Specifically, paper A details the MC model discussed in Chapter 3. Paper B investigates the effect of MC on the sum rate of MU-MIMO systems for different inter-element spacing at the BSA.

Chapter 2

Mutual Coupling in Massive MIMO Systems

In this chapter, a brief overview of the impact of MC in Massive MIMO systems, and an overview of computational approaches for the analysis of MC, are presented. For a more general discussion on the electromagnetic and circuit-theoretic aspects of MC, the reader is referred to [26].

2.1 Impact of Mutual Coupling

The effect of antenna array MC, which alters the impedance and radiation characteristics of an isolated antenna element, plays an important role in terms of the element selection, array design and overall functioning of a (Massive) MU-MIMO system. Obviously, an important question arises here as: *How adverse is the effect of MC on the performance of a Massive MIMO system?* This question is addressed by analyzing the impact of different system variables associated with array MC effects.

An example of an important design parameter for antenna arrays for Massive MIMO applications, is the embedded element gain variation, caused by MC and the edge effect due to a finite array dimension. In an infinite array, each antenna effectively sees the same surroundings. Consequently, the embedded element gain (in any direction) is equal for all elements. Moreover, in a multipath channel, the embedded element gain should ideally be omnidirectional to efficiently receive the signal components arriving from different directions [36]. Large variations of the embedded element gain within an antenna array or overly-directive embedded element gain patterns may degrade the sum-rate performance of a Massive MIMO system or introduce user unfairness, depending on the choice of the applied linear processing algorithms, as discussed in [36]. In a finite array, the location of an antenna within an array determines its embedded element gain. Hence, depending on the considered element and array configuration, significant embedded gain variations between the

elements may appear.

Let us now, for example, consider two elements commonly used in theoretical analyses and experiments involving the (Massive) MU-MIMO systems — dipoles and patch antennas. A dipole antenna generates an omnidirectional radiation pattern in the H-plane, while a patch antenna is more directive. By looking at the isolated element only, one might assume that the characteristics of the isolated element will translate to the array environment, by which a dipole array would exhibit a smaller embedded gain variation compared to that of an array of patch antennas. Hence, from the embedded gain variation perspective, a dipole antenna might initially seem a more suitable candidate-element for the deployment in antenna arrays for Massive MIMO applications. However, the analysis performed in [36] indicates the opposite. Dipoles embedded in an array environment exhibit stronger mutual interactions compared to patches, which has a more destructive influence on the embedded element gain variation and the omni-directionality of the isolated element. Hence, perhaps counter-intuitively, patch arrays appear a better choice from this perspective. In the same paper, the effect of the embedded gain variation on the user rate has been analyzed, showing the sensitivity of a Massive MIMO system to the angle of arrival with regards to user locations.

Another important parameter of an antenna array related to MC is the embedded radiation (decoupling) efficiency, defined in [35, Ch. 3.3.3] assuming lossless antennas. Embedded element efficiency reflects the fact that, in a multi-port system, a fraction of the signal on each port is coupled to all other (terminated) ports [35, p. 84]. Moreover, it includes the mismatch at that particular port. Hence, the ability of the port (antenna) to radiate the accepted power into space is degraded with increased mismatch or MC to other ports. As such, embedded element efficiency represents a fundamental limitation for MIMO systems [35, 11.3.2], [37], particularly in the context of envisioned large antenna arrays for Massive MIMO applications. Similarly, the active reflection coefficient (ARC) [38] is an important design variable as it describes the induced mismatch at the antenna due to MC from other actively driven phased-array antennas.

In this context, it can be reasoned that the performance of a Massive MIMO system may benefit from the optimal element selection in terms of low inter-element coupling. A promising candidate to meet such requirement could be a patch antenna [39, 40]. Possibly, the design of an element could benefit from various decoupling techniques discussed in [41] and compared in Table 1 of [42]. Alternatively, MC in previously fabricated antenna arrays could be reduced by adding a metamaterial-inspired superstrate, as described in [42], allowing a simple technology transfer.

Finally, the fact that the signals at different ports are not completely independent (thus being correlated), i.e., the signal correlation [35, 3.3.4], contributes to the system performance degradation. Low correlation between the ports improves the performance of a MIMO system [41]. However, the link between the correlation and

MC is not obvious, as demonstrated in Fig. 5 of [41], which shows the correlation between two dipoles for different inter-element spacings. The figure indicates that, depending on the spacing, MC can both increase or decrease the correlation compared to the case where the effect of MC is not considered. Surprisingly, this result implies that, for a given element selection, a certain spacing might exist for which the effect of MC actually benefits the system performance through the correlation mechanism.

A systematic review of MC in MIMO systems, including an overview of the decoupling techniques used in Massive MIMO, and the impact of MC on the system performance, is given in [41]. Regarding the system performance, four aspects have been analyzed, namely the diversity gain, channel capacity, error rate and spectral regrowth.

A diversity is a communication concept which utilizes more than a single antenna in the receiving mode, where each diversity antenna is part of a separate receiver and receives a copy of the transmitted signal [43]. The receive antennas may exploit spatial diversity, being spaced apart by some distance, or polarization diversity, being collocated but receiving a different polarization. By combining the receiving signals in a proper way, the probability of fading can be reduced [35, 3.4]. Additionally, the signal-to-noise ratio (SNR) of a combined signal should ideally be considerably higher compared to the SNR of any of the diversity antennas [43]. The relative increase of the SNR compared to the SNR of a single diversity antenna is called the diversity gain. In the context of MC, the diversity gain, as well as the channel capacity and error rate performance, depend on both the embedded efficiency and correlation [41]. Hence, the systemic impact of MC is not straightforward.

Therefore, in conclusion, MC in Massive MIMO systems appears as a predominantly destructive influence, except for certain inter-element spacing(s), for which it may improve the system performance [41]. For a given antenna selection, finding such a spacing, or, in general, array configuration, which yield the optimal system performance, often requires several design iterations, as discussed in Subsec. 1.3.1. Such a strategy accentuates the importance of using the computationally-efficient approaches for the modeling of antenna arrays including the MC.

2.2 Analysis of Mutual Coupling

In the preceding subsection, the impact of MC on various aspects of a Massive MIMO system has been discussed, showing the importance of its evaluation and inclusion in the design scheme of the system illustrated in Fig. 1.3. In this subsection, different strategies for the analysis of MC are discussed.

When the geometry of an element permits, MC in terms of the array impedance matrix can be straightforwardly described in closed form. One such example is the mutual impedance between a pair of dipoles [44, 6.2], an element commonly used in

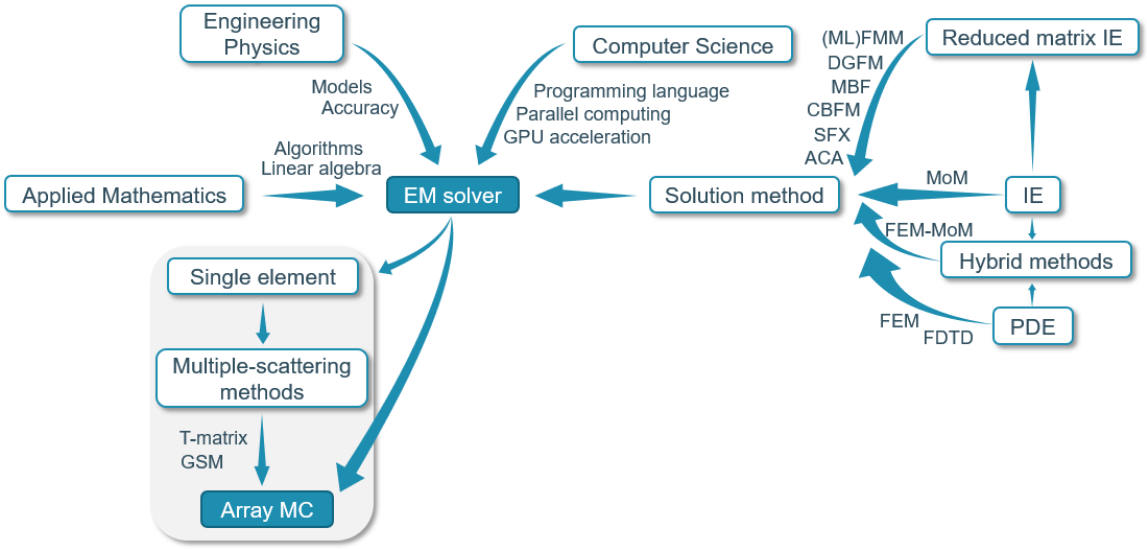

Figure 2.1: Overview of numerical simulation software for the analysis of antenna array mutual coupling.

the analyses of MIMO systems. The impedance matrix of a dipole array obtained in this way can be used, for example, to describe MC in the BSA [45], to calculate the channel matrix in a non-line-of-sight (NLoS) propagation environment involving dipole scatterers [46], or be applied in the self-interference cancellation scheme in full-duplex MIMO systems [47]. However, MC generally needs to be evaluated numerically by using an EM solver, as described in Fig. 2.1. The EM solver is a complex tool which coordinates the concepts from different disciplines, e.g., applied mathematics, computer science and engineering physics, to obtain an accurate solution for the MC in a reasonable time period. While the former two form the computational backbone of the solver, the engineering aspects including the meshing, material and port definitions, boundary conditions and various simulation parameters, are user-controlled and influence the solution time and accuracy.

Regarding the solution method, two main solution strategies can be distinguished, based on the mathematical description of Maxwell's equations in the integral equation (IE) form or the partial differential equation (PDE) form. The former includes the method of moments (MoM), while the latter include the finite-element method (FEM) or the finite-difference time-domain (FDTD) method. Alternatively, a hybrid approach can be used, in which the antenna geometry is divided in different regions, and each region is solved using the most appropriate solution method for that region. These fundamental concepts, also known as the full-wave computational electromagnetics (CEM) methods [48, Ch. 4], may provide an accurate solution for the MC, although they might suffer from poor computation time and memory scaling when electrically large antenna problems need to be analyzed. Therefore, various

Table 2.1: Computational complexities of several IE-based methods, based on the analyses in indicated references. Here, N is the number of elements, N_i is the number of unknowns per element while $N_\mathrm{x} = N \times N_\mathrm{i}$ is the total number of unknowns.

Method	**Run time** $\mathcal{O}(\cdot)$	**Memory** $\mathcal{O}(\cdot)$
MoM [57]	N_x^3	N_x^2
MLFMM [57]	$N_\mathrm{x} \log^2 N_\mathrm{x}$	$N_\mathrm{x} \log N_\mathrm{x}$
DGFM [58]	$N \times N_\mathrm{i}^3$	N_i^2
CBFM [58]	N^6	$2N_\mathrm{i}^2 + N^4$
ACA [56][1]	${N_\mathrm{x}}^{4/3} \log N_\mathrm{x}$	${N_\mathrm{x}}^{4/3} \log N_\mathrm{x}$

concepts aimed at reducing the computational complexity of the problem have been implemented. In the context of IE-based solutions, these concepts include the multilevel fast multipole method (MLFMM) [49,50], the domain Green's function method (DGFM) [51], the macro basis function approach (MBF) [52], the characteristic basis function method (CBFM) [53,54], the synthetic function approach (SFX) [55] or the adaptive cross approximation algorithm (ACA) [56]. The computational complexities of several IE-based techniques are compared in Table 2.1. The solution for the antenna array MC can be obtained in two ways, as shown in Fig. 2.1, i.e., by directly solving for the entire antenna array, or alternatively, by solving first for a single element in isolation, prior to accounting for the MC by modeling the interactions between different array elements or, in general, between the smaller partitions of the entire array problem. The representatives of the latter approach are termed in literature as the domain-decomposition methods (DDMs). The use of the DDM methods may significantly reduce the number of unknowns in the considered problem compared to when the array geometry is treated as a whole. In general, the computational scaling of the DDM methods is impacted by the domain discretization, i.e., the number of the unknowns per domain, as it can be appreciated in the computational complexities of the DGFM or the CBFM listed in Table 2.1. A special subset of the DDM methods involves the multiple-scattering methods, which treat the effect of MC by modeling the relations between the incoming and outgoing expansion waves in an antenna array. The scaling of the multiple-scattering-based methods is independent of the element discretization in the sense that such methods scale only with the number of the array elements.

Based on the modeling principles for MC, different multiple-scattering strategies can be distinguished. For example, the T-matrix method [59,60] relates the spherical wave expansion (SWE) of an incoming wave at the scatterer, with the SWE of an outgoing (scattered) wave. Similarly, the generalized scattering matrix (GSM) approach [61] models both the field effects using the SWE and the reflections at the

[1]The complexity of the ACA algorithm depends on the problem size, as discussed in [56]. The listed complexity corresponds to "moderately-sized problems".

antenna ports, reflecting the physical nature of MC due to the external excitation. Alternatively, in the expansion wave concept (EWC), the interactions between the elements are modeled by using the analytical Green's function approximation for stratified dieletric media [62,63]. Moreover, the principles of multiple scattering may be used to compute the characteristic modes in the presence of MC [64], which might provide a useful physical insight into the characteristic-mode-inspired antenna design for Massive MIMO applications [65].

Chapter 3

Fast Characterization of Sparse-Array Mutual Coupling

In Ch. 1 an iterative co-design strategy for antenna arrays for Massive MIMO applications has been outlined, as e.g., illustrated in Fig. 1.3. A similar strategy can be used for the design and synthesis of sparse arrays [66, 67], a promising architecture for Massive MIMO BSAs [9]. Such a strategy requires the assessment of MC in each design iteration, used as the input for the next iteration. In the context of large arrays for Massive MIMO applications, the conventional full-wave analysis of MC may become prohibitively expensive due to increased electrical dimensions of the array. Hence, various alternative approaches to alleviate the computational effort required to analyze the MC have been mentioned in Ch. 2. Particularly, the approaches based on the concept of multiple scattering, which require the full-wave solution of only a single antenna element rather than the full-wave analysis of the entire array, represent an intriguing prospect in this context. Such approaches scale with the number of elements rather than the number of subsectional basis functions, which may offer significant rewards in terms of the overall computation time and memory requirements. Thus, the focus of this chapter is on the development and analysis of a novel computationally-efficient method for the analysis of sparse-array MC, which is based on the concept of multiple scattering and employs only the simulated sampled field data of an isolated element. The effect of MC is computed by cascading the expansion-wave responses of all array elements, i.e., by modeling the relations between the incoming and outgoing waves in the multiple-scattering array environment. The contents of this chapter are based on Paper A.

3.1 Model Description

A classical MoM system description $\boldsymbol{ZJ} = \boldsymbol{V}$ relates the surface currents $\boldsymbol{J}$ to voltages $\boldsymbol{V}$ through the array impedance matrix $\boldsymbol{Z}$. It is often convenient to describe

this system using a block-based structure, where each block may be associated with the domain of one element. Then, the impedance matrix can be decomposed into its on-diagonal and off-diagonal block-constituents as $\boldsymbol{Z} = \boldsymbol{Z}_{\text{on}} + \boldsymbol{Z}_{\text{off}}$, where $\boldsymbol{Z}_{\text{on}}$ contains the intra-element coupling blocks, denoted as $\boldsymbol{Z}_{mm}$, while $\boldsymbol{Z}_{\text{off}}$ contains the inter-element coupling blocks $\boldsymbol{Z}_{mm'}(m \neq m')$. Then, the solution for the $m-$th surface current in iteration $q \geq 1$ may be obtained iteratively, for example using the Jacobi method as [68]

$$\boldsymbol{J}_m^{(q)} = \boldsymbol{Z}_{\text{on},mm}^{-1} \left(\boldsymbol{V}_m - \sum_{m'=1,\, m' \neq m}^{N} \boldsymbol{Z}_{\text{off},mm'} \boldsymbol{J}_{m'}^{(q-1)} \right), \tag{3.1}$$

where $\boldsymbol{Z}_{\text{on},mm}^{-1} \boldsymbol{V}_m = \boldsymbol{J}_m^{(0)}$ is the current in isolation.

Based on the reciprocity between the surface currents and electric fields, a similar iterative scheme exists in terms of the electric fields as [34, 69]

$$\underline{\boldsymbol{E}}_m^{(q)} = \underline{\boldsymbol{E}}_m^{(0)} + \sum_{m'=1,\, m' \neq m}^{N} \underline{\underline{\boldsymbol{E}}}_{mm'}^{\text{s}(0)} \underline{\boldsymbol{E}}_{m'}^{(q-1)}. \tag{3.2}$$

Here, $\underline{\boldsymbol{E}}_m^{(0)}$ is the field of an isolated element m, and $\underline{\underline{\boldsymbol{E}}}_{mm'}^{\text{s}(0)}$ is a dyad which transforms the electric field of element m', due to a unit-amplitude source, into the field scattered by element m [34]. Note that, for $q < 0$, $\boldsymbol{J}_m^{(q)} = \boldsymbol{0}$ and $\underline{\boldsymbol{E}}_m^{(q)} = \boldsymbol{0}$.

According to the Schelkunoff's equivalence principle, tangential components of the field at any fictitious surface of a volume which completely encloses the element, provide a complete description for the radiated or scattered field of that element. For convenience, we may define a spherical surface for which the tangential unit vectors correspond to $\hat{\boldsymbol{\theta}}$ and $\hat{\boldsymbol{\phi}}$. Then, it is reasonable to associate the local spherical coordinate systems with all array elements. In a scattering environment, we may associate the primed system with the source m', and the unprimed system with the scatterer m, as illustrated in Fig. 3.1. The equivalent source field restricted to the tangential field components at the spherical surface around m' is denoted as $\underline{\boldsymbol{E}}_{m'}^{(q-1)}|_{\theta',\phi'}$. Moreover, the dyad is defined as

$$\underline{\underline{\boldsymbol{E}}}_{mm'}^{\text{s}(0)} = \begin{bmatrix} E_{mm'_{\theta,\theta'}}^{\text{s}(0)} & E_{mm'_{\theta,\phi'}}^{\text{s}(0)} \\ E_{mm'_{\phi,\theta'}}^{\text{s}(0)} & E_{mm'_{\phi,\phi'}}^{\text{s}(0)} \\ E_{mm'_{r,\theta'}}^{\text{s}(0)} & E_{mm'_{r,\phi'}}^{\text{s}(0)} \end{bmatrix}. \tag{3.3}$$

The columns of the dyad contain the transforms which relate the $\hat{\boldsymbol{\theta}}'$ and $\hat{\boldsymbol{\phi}}'$-polarized fields emanating from element m' to the spherical components of the induced scattered field at the surface around element m. Instead of restricting the field of source m' to the tangential components at its own spherical surface, we can first project the

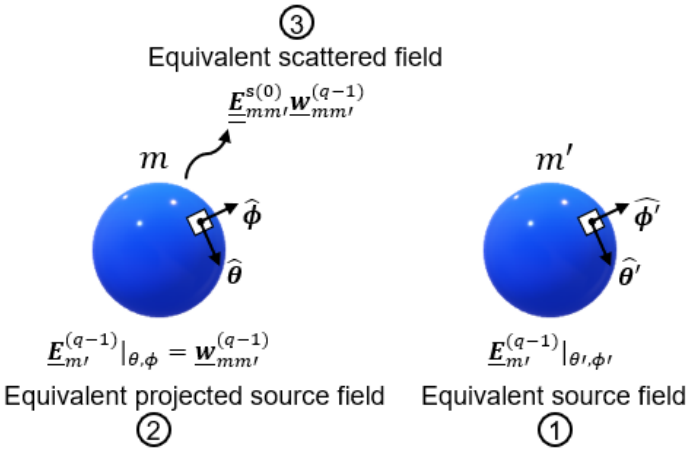

Figure 3.1: Scattering by element m according to the Schelkunoff's equivalence principle. Both elements are replaced by the equivalent field distribution on the surface of a sphere which circumscribes that element completely. The spheres of the two elements must not overlap.

components of the source field onto the spherical surface of element m, as illustrated in Fig. 3.1. In notation, $\underline{\boldsymbol{E}}^{(q-1)}_{m'}|_{\theta',\phi'}$ becomes $\underline{\boldsymbol{E}}^{(q-1)}_{m'}|_{\theta,\phi} = \underline{\boldsymbol{w}}^{(q-1)}_{mm'} = \left[w^{(q-1)}_{mm',\theta} \quad w^{(q-1)}_{mm',\phi}\right]^T$, where $|_{\theta,\phi}$ indicates the restriction to the (unprimed) coordinate system of element m. Consequently, the primes in the angular components of the dyad in (3.3) are removed. Finally, the projected source field of element m' induces the scattered field at the spherical surface of element m, $\underline{\underline{\boldsymbol{E}}}^{s(0)}_{mm'}\,\underline{\boldsymbol{E}}^{(q-1)}_{m'}$, which modifies the total field distribution of element m in iteration q, as suggested by Eq. 3.2.

Similarly, instead of iterating the total field of element m as described by Eq. (3.2), one might consider updating the projection of this field onto the spherical surface of element p in the same notation as given in Fig. 3.1, which can be described as

$$\underline{\boldsymbol{w}}^{(q)}_{pm} = \underline{\boldsymbol{E}}^{(q)}_{m}|_{\theta,\phi} = \underline{\boldsymbol{E}}^{(0)}_{m}|_{\theta,\phi} + \sum_{m'=1,\, m'\neq m}^{N} \left(\underline{\underline{\boldsymbol{E}}}^{s(0)}_{mm'}\,\underline{\boldsymbol{w}}^{(q-1)}_{mm'}\right)|_{\theta,\phi}\,, \tag{3.4}$$

where θ and ϕ relate to the coordinate system of element p.

By assuming a far-field distance between the elements, the projection of the field of element m' onto the spherical surface of element m can be reduced to a single direction of incidence. Then, the projected vector field $\underline{\boldsymbol{w}}^{(q-1)}_{mm'}$ reduces to a vector $\underline{\check{\boldsymbol{w}}}^{(q-1)}_{mm'} \in \mathbb{C}^{2\times 1}$. Consequently, the far-field equivalent of (3.2) is

$$\underline{\boldsymbol{F}}^{(q)}_{m} = \underline{\boldsymbol{F}}^{(0)}_{m} + \sum_{m'=1,\, m'\neq m}^{N} \underline{\underline{\boldsymbol{F}}}^{s(0)}_{mm'}\,\underline{\check{\boldsymbol{w}}}^{(q-1)}_{mm'}\,. \tag{3.5}$$

Here, $\underline{\boldsymbol{F}}_m^{(0)}$ and $\underline{\underline{\boldsymbol{F}}}^{\mathrm{s}(0)}_{mm'} \in \mathbb{C}^{2\times 2}$ are the far-field equivalents of $\underline{\boldsymbol{E}}_m^{(0)}$ and $\underline{\underline{\boldsymbol{E}}}^{\mathrm{s}(0)}_{mm'}$, respectively.

Similarly, for the far-field case in Eq. (3.5), the currents at the antenna terminals may be related to $\underline{\check{\boldsymbol{w}}}^{(q-1)}_{mm'}$ as

$$I_m^{(q)} = I_m^{(0)} + \sum_{\substack{m'=1 \\ m'\neq m}}^{N} \boldsymbol{I}^{\mathrm{i}(0)}_{mm'} \underline{\check{\boldsymbol{w}}}^{(q-1)}_{mm'}, \tag{3.6}$$

where $I_m^{(0)}$ is the terminal current in isolation while $\boldsymbol{I}^{\mathrm{i}(0)}_{mm'} = \begin{bmatrix} I^{\mathrm{i}(0)}_{mm'_\theta} & I^{\mathrm{i}(0)}_{mm'_\phi} \end{bmatrix} \in \mathbb{C}^{1\times 2}$ contains the induced terminal currents at element m due to unit-amplitude $\hat{\boldsymbol{\theta}}$ and $\hat{\boldsymbol{\phi}}$-polarized plane waves emanating from direction $\boldsymbol{r}_{mm'} = \boldsymbol{r}_m - \boldsymbol{r}_{m'}$, where $\boldsymbol{r}_m$ and $\boldsymbol{r}_{m'}$ are the reference points of elements m and m', respectively. When the terminal currents are known, the S-parameters can be extracted straightforwardly.

The field-update process in Eq. (3.4) is performed as follows. The terms $\underline{\boldsymbol{E}}_m^{(0)}|_{\theta,\phi}$ and $(\underline{\underline{\boldsymbol{E}}}^{\mathrm{s}(0)}_{mm'}\, \underline{\boldsymbol{w}}^{(q-1)}_{mm'})|_{\theta,\phi}$, require the evaluation of the radiated or scattered field of element m, respectively, at the sphere of element p, restricted to its angular components in the $p-$th coordinate system. The electric field terms in Eq. (3.4) can for example be decomposed into a SWE [70, Ch. 3.10]. By using the SWE, the electric field can in theory be determined with reasonable accuracy at any point outside the source region[1]. Assuming the far-field distance between elements p and m, the effect of MC can be reduced to a single plane wave with mutually-orthogonal polarization, traveling in the direction $\boldsymbol{r}_{pm} = \boldsymbol{r}_p - \boldsymbol{r}_m$, i.e., along the direct path between the elements' reference points $\boldsymbol{r}_p$ and $\boldsymbol{r}_m$, as detailed in Paper A. This approach is termed as "SW-PW" [34, 69]. When the elements are in each other's far fields, the selection of the antenna reference point is rather arbitrary. In the implementation described in Paper A, the antenna reference point is placed in the center of a minimum sphere which envelops all the radiating parts of the antenna.

By using the "SW-PW" approach, the complex magnitudes of the vector components of the plane wave are determined by projecting the SWE-based $\hat{\boldsymbol{\theta}}'$ and $\hat{\boldsymbol{\phi}}'$ components of element m onto the spherical vectors $\hat{\boldsymbol{\theta}}$ and $\hat{\boldsymbol{\phi}}$ at the reference point $\boldsymbol{r}_p$ of element p. Consequently, the scattered field at element p can be determined by scaling the simulated scattered field due to a unit-amplitude plane wave traveling in the direction $\boldsymbol{r}_{pm}$ with the corresponding complex magnitude of the plane wave. The details on the theoretical background of the discussed MC model, including the transformation from the SWE to a single plane wave, can be found in Paper A.

The required simulated data of the isolated element include the radiated far field and terminal current due to the voltage source excitation of 1 V, and a set of scattered far fields and induced terminal currents due to plane waves of 1 V/m impinging

[1]The accuracy of the SWE field representation w.r.t. the type of the sampled field data from which the SWE is determined (near or far-field data), and the distance of the observation point in which the field is calculated from the source, is discussed in [34, p. 4].

from several directions. These data can be obtained straightforwardly using any available EM field solver and need to be computed only once. Note that, when the characteristics of an isolated element are known, arbitrary element orientations and array configurations can be modeled through relatively simple manipulations of the available isolated element data. Specifically, the SWE modal content of the isolated element can be appropriately modified according to the element tilt (rotation), while the scattered fields (and terminal currents) for unknown directions can be interpolated from the dataset containing the scattered fields and currents for known (simulated) directions of incident plane waves. In the next section, the performance of the method is analyzed in terms of the accuracy and run time, and compared to that of a commercially available MoM-based "FEKO" solver.

3.2 Numerical Analysis

To illustrate the applicability of the method for sparse antenna array modeling, ARC and far-field EEP results are obtained for various excitations of the array of planar inverted-F antennas (PIFAs) shown in Fig. 3.2 (the "triangle edge length" mesh setting in FEKO is set at $\lambda_0/50$). Active reflection coefficients for center (i) and corner elements (j) of this array are plotted in Fig. 3.3, in the case of: (a) the uniformly-excited array and (b) scanned array ($\theta_s = 60°$, $\phi_s = 0°$). EEPs of the center element i at the $\theta = 90°$ plane [plot labels (a) and (b)], and the corner element j at the $\phi = 0°$ plane [plot labels (c) and (d)] of the 9×9 PIFA array shown in Fig. 3.2, are plotted in Fig. 3.4.

Both the ARC plots in Fig. 3.3 and the EEP plots in Fig. 3.4 show a good agreement between the results using this model and the MoM-based results using FEKO. Specifically, the method under consideration has been able to replicate well the MoM-based fields in different observation planes (including the rapid phase oscillations in the azimuth plane) and the ARCs for different scanning conditions. Both figures include the results for an isolated element to illustrate the non-negligible effect of MC, where IEP denotes the *isolated element pattern*. Although the studied example may lack the practical relevance for various applications due to the appearance of the grating lobes owing to a relatively large inter-element spacing ($0.8\lambda_0$), and due to having the less favorable ARC for broadside radiation, the results shown in Figs. 3.3 and 3.4 demonstrate the robustness of the method to different excitation conditions manifested both in terms of the port parameters and radiated fields. Similarly, the method can be used for the analysis of ISAs, as shown in Paper A.

The analyses of the convergence[2] and computational complexity including the run-time comparison between this method and FEKO's MoM or MLFMM-based solvers

[2]The convergence analysis includes the comparison of the Jacobi-based iteration given by Eq. (3.4) and the alternative Gauss-Seidel-based iteration, indicating the strong dependency of the convergence on the selection of the iterative technique.

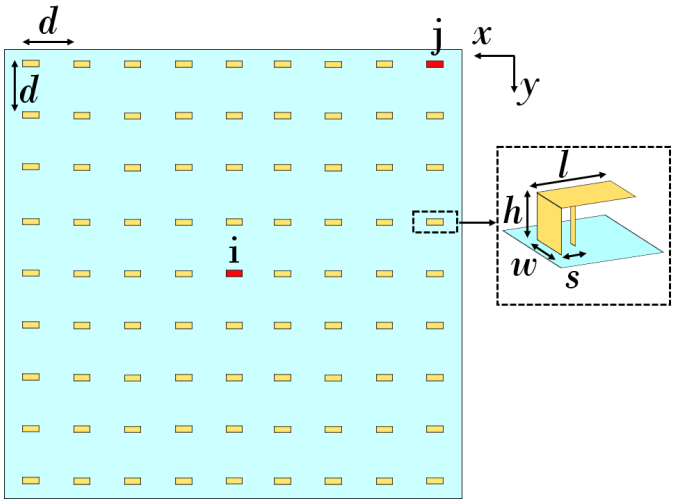

Figure 3.2: Layout of a 9×9 regular PIFA array (with infinite ground plane in light blue): $f_0 = 28\,\text{GHz}$, $l = 2.14\,\text{mm}$, $w = 0.5\,\text{mm}$, $h = 0.71\,\text{mm}$, $s = 0.39\,\text{mm}$, $d = 0.8\lambda_0 = 8.57\,\text{mm}$. EEPs are computed for the center element labeled "i" and the corner element labeled "j" (see also [34, Fig. 6]).

for different array types and configurations, is detailed in Paper A. Specifically, the method under consideration has been shown to significantly outperform FEKO's run times required to compute all EEPs in antenna arrays containing up to more than a hundred of PIFA elements shown in Fig. 3.2. For example, the run-time reduction is in the order of factor 25 for the 11×11 array of PIFA elements shown in Fig. 3.2. For fixed array sizes in terms of the number of elements, the run-time savings may be increasingly more favorable for this method when the analysis involves more complex elements which require many basis functions per element. The growing element complexity hinders the run-time performances of the MoM or MLFMM-based solvers, while the run-time performance of this method is largely unaffected if the scaling of the method is dominated by the number of elements (the other variable being the number of iterations required to reach the solution, which a.o., depends on the element size, as observed in Paper A).

As mentioned in the introductory remarks of this chapter, the development of this model has been mainly motivated by the search for an efficient alternative to full-wave techniques in the context of the rapid assessment of MC, required e.g., for the sequential design or synthesis of sparse arrays for Massive MIMO applications. The developed model presented in this chapter fits these prerequisites. It can be used to analyze the MC in arbitrary antenna arrays with some arbitrary element, in terms of both the electric fields and the S-parameters. Moreover, it can be used with different excitation schemes (embedded excitation or an actively-driven array). Additionally, it is suitable for use in the sequential array design applications while

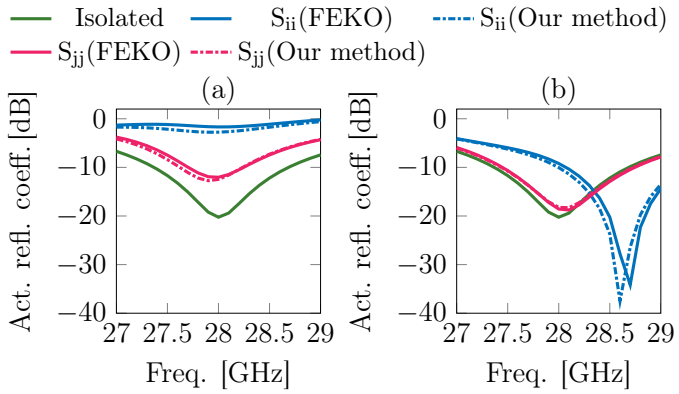

Figure 3.3: Active reflection coefficients for the center and corner elements i and j of the 9×9 PIFA array shown in Fig. 3.2 ($f_0 = 28\,\text{GHz}$, $d = 0.8\lambda_0$) as a function of frequency: (a) Uniformly-excited array. (b) Scanned array ($\theta_s = 60°, \phi_s = 0°$) (see also [34, Fig. 10]).

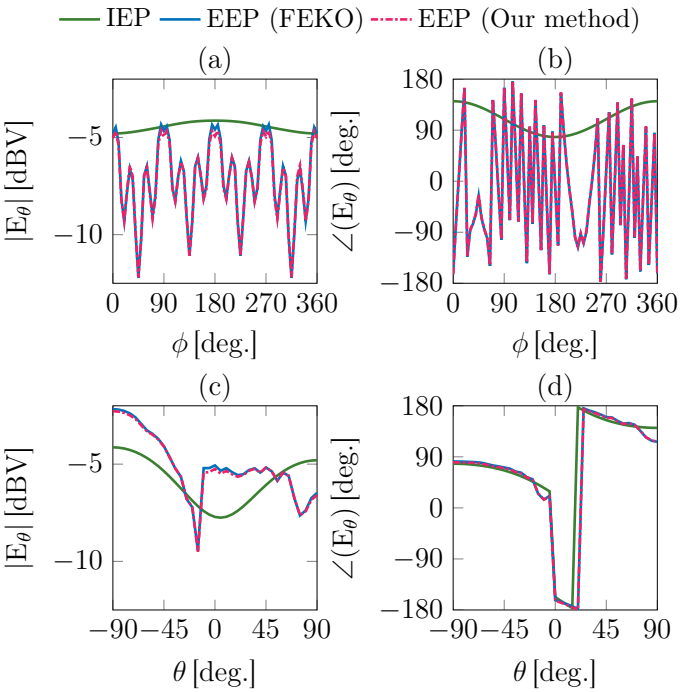

Figure 3.4: EEPs of the center element i at the $\theta = 90°$ plane (a)-(b), and the corner element j at the $\phi = 0°$ plane (c)-(d) of the 9×9 PIFA array shown in Fig. 3.2 ($f_0 = 28\,\text{GHz}$, $d = 0.8\lambda_0$) (see also [34, Fig. 11]).

varying the array lattice or excitation, since the MC in each design iteration can be efficiently determined by using the methodology which reuses the data of an isolated element, thereby requiring no further full-wave simulations. The method is primarily intended for the analysis of sparse array configurations owing to its far-field character manifested in approximating the SWE-based incident field as a single plane wave. Moreover, the representing surfaces of any two array elements according to the Schelkunoff's equivalence principle discussed in Sec. 3.1, which correspond to the minimum spheres of these elements in this implementation, must not overlap. Several possibilities to improve the applicability of the method to arrays with relatively small spacings are discussed in Ch. 5.

Chapter 4

Mutual Coupling in LoS MU-MIMO Systems

In this chapter, the analysis of the MC obtained using the method described in Ch. 3 is incorporated into the sum-rate model of the downlink LoS MU-MIMO system, presented in Paper B. The use of the method discussed in Ch. 3 to analyze the MC may significantly reduce the required computational costs compared to when the conventional full-wave techniques are used, particularly when large array configurations need to be (rapidly) analyzed. In the combined model, MC in terms of the EEPs and the S-matrix of the BSA is used to model the propagation effects in the LoS channel. Such approach represents a more complete and accurate description of the LoS MU-MIMO system compared to the analyses traditionally performed within the information-theory communities. In such analyses, the effects of the MC are often underestimated by assuming idealized antenna elements with no MC between them or by considering the fictitious isotropic radiators, which might lead to erroneous conclusions when the effects of MC cannot be ignored.

In the Massive MIMO systems which are governed by the laws and principles of both the electromagnetic and information theories, the relation between the given BSA configuration and the accomplished system performance may not be straightforward and intuitive. This performance can e.g., be analyzed in terms of the achievable sum rate, which in turn may be used to evaluate the spectral and energy efficiencies, two of the most important indicators of the performance of the Massive MIMO system [9, 11]. These performance metrics provide the valuable feedback in the context of the iterative co-design strategy for the Massive MIMO BSAs discussed in 1.3.1. Thus, the aim of this chapter is to analyze the use potential of the combined Paper A-Paper B model for the Massive MIMO BSA design applications, by evaluating its accuracy in terms of the sum rate compared to the model presented in Paper B, which uses the MC data obtained by using the MoM-based solver.

4.1 Network Model

A two-port network model of a downlink MU-MIMO system with M BSA antennas and K single-antenna UEs is illustrated in Fig. 4.1. Mathematically, this system is

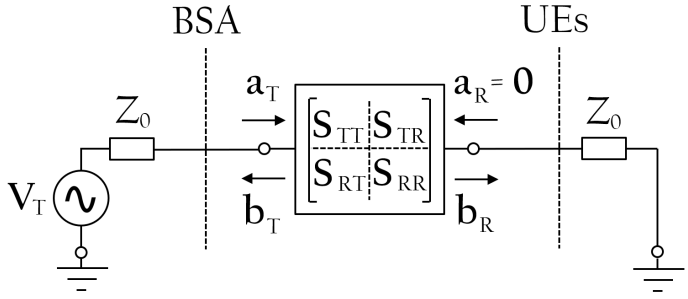

Figure 4.1: Network model of a downlink MU-MIMO system (see also [71, Fig. 1].)

described as

$$\begin{bmatrix} \boldsymbol{b}_{\mathrm{T}} \\ \boldsymbol{b}_{\mathrm{R}} \end{bmatrix} = \begin{bmatrix} \boldsymbol{S}_{\mathrm{TT}} & \boldsymbol{S}_{\mathrm{TR}} \\ \boldsymbol{S}_{\mathrm{RT}} & \boldsymbol{S}_{\mathrm{RR}} \end{bmatrix} \begin{bmatrix} \boldsymbol{a}_{\mathrm{T}} \\ \boldsymbol{a}_{\mathrm{R}} = \boldsymbol{0} \end{bmatrix}. \tag{4.1}$$

Here, subscripts "T" and "R" represent the transmit and receive ports, respectively. The transmit ports are excited through a Thévenin voltage source with an RMS voltage V_{T} and the source impedance Z_0. Furthermore, $\boldsymbol{a}$ and $\boldsymbol{b}$ represent the incoming and outgoing (reflected) power wave vectors w.r.t. the ports of the network, respectively. Moreover, $\boldsymbol{S}_{\mathrm{TT}} \in \mathbb{C}^{M\times M}$ and $\boldsymbol{S}_{\mathrm{RR}}$ ($\in \mathbb{C}^{K\times K}$, assuming the single-antenna UEs) denote the S-matrices of the BSA and UEs, respectively. Similarly, $\boldsymbol{S}_{\mathrm{RT}} \in \mathbb{C}^{K\times M}$ and $\boldsymbol{S}_{\mathrm{TR}} = \boldsymbol{S}_{\mathrm{RT}}^{T}$ contain the interactions between the BSA and UEs. Assuming a perfectly matched receiver, no power is reflected back towards the BSA at the UEs' terminals, thus, $\boldsymbol{a}_R = 0$. Additionally, in most practical scenarios, MC between the UEs can be neglected due to a relatively large (electrical) distance between them. Consequently, $\boldsymbol{S}_{\mathrm{RR}}$ is the diagonal matrix.

In a LoS environment, the direct wave from the transmit array becomes the dominant component in the channel[1]. Physically, this wave may be viewed as being composed of the (weighted) EEPs of all elements of the transmit array antenna. Consequently, the channel matrix $\boldsymbol{H} = \boldsymbol{S}_{\mathrm{RT}}$ can be approximated through the EEPs of the transmit antennas, $\boldsymbol{E}^{\mathrm{emb}}$, generated using the Thévenin voltage source equivalent, as illustrated in Fig. 4.2. It follows from Eq. (4.1) that the power wave b_{R_k}, corresponding to user k, is proportional to both the $\boldsymbol{E}^{\mathrm{emb}}$ and a_{T} terms as [35, Ch. 2]

$$|b_{\mathrm{R}_k}| \propto \left| \hat{\boldsymbol{l}}_k \cdot \sum_{m=1}^{M} a_m^T \boldsymbol{E}_m^{\mathrm{emb}}(r_k, \theta_k, \phi_k) \right|. \tag{4.2}$$

[1] A model of a NLoS channel is discussed in [9, Ch. 4].

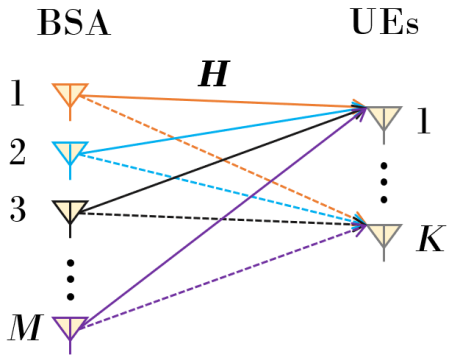

Figure 4.2: Channel matrix $\boldsymbol{H}$ of a downlink LoS MU-MIMO system with M transmit antennas and K single-antenna users. The arrows indicate the embedded element patterns of the transmit antennas.

Here, $a_{\mathrm{T}} = V_{\mathrm{T}}/(2\sqrt{\Re\{Z_0\}})$ [72, Ch. 2], while $\hat{\boldsymbol{l}}_k$ and (r_k, θ_k, ϕ_k) are the polarization vector and spherical coordinates of user k, respectively.

4.2 Sum Rate

To estimate the sum rate, the channel-noise model for the downlink LoS channel is used, as described in [73, Sec. 4.3]. This model assumes that the dominant source of noise in the system is from the channel, therefore, the receiver noise can be neglected [74]. Consequently, the power wave vector $\boldsymbol{b}_{\mathrm{R}} \in \mathcal{C}^{K\times 1}$ can be expressed as

$$\boldsymbol{b}_{\mathrm{R}} = \boldsymbol{S}_{\mathrm{RT}}\boldsymbol{a}_{\mathrm{T}} + 2\Re\{Z_0\}^{-1/2}\boldsymbol{n}, \tag{4.3}$$

where $\boldsymbol{n} \in \mathcal{C}^{K\times 1}$ is the additive white Gaussian noise (AWGN) vector. Moreover, the constraint is placed on the total radiated power P_{tot}, according to Eq. (9) of [73]. For example, P_{tot} can be chosen to guarantee a certain SNR at the users. Then, the downlink capacity is expressed as

$$\begin{aligned} C = \max_{\boldsymbol{K}_{a_{\mathrm{T}}}} \ & \log_2\left[\det\left(\boldsymbol{I}_K + \frac{1}{N_0}\boldsymbol{H}\boldsymbol{K}_{a_{\mathrm{T}}}\boldsymbol{H}^H\right)\right], \\ \text{s.t. } & \operatorname{trace}\left(\boldsymbol{K}_{a_{\mathrm{T}}}\left(\boldsymbol{I}_M - \boldsymbol{S}_{\mathrm{TT}}^H\boldsymbol{S}_{\mathrm{TT}}\right)\right) \le P_{\mathrm{tot}}, \end{aligned} \tag{4.4}$$

where $\boldsymbol{K}_{a_{\mathrm{T}}} \in \mathbb{C}^{M\times M}$ is the diagonal covariance matrix of $\boldsymbol{a}_{\mathrm{T}}$, N_0 is the noise power at the UE terminal, while $\boldsymbol{I}_K \in \mathbb{C}^{K\times K}$ and $\boldsymbol{I}_M \in \mathbb{C}^{M\times M}$ are the identity matrices. Moreover, $\{\,\cdot\}^H$ denotes the conjugate transpose operator. Only the BSA possesses the channel state information. By equally allocating the power among the BSA antennas, $\boldsymbol{K}^*_{a_{\mathrm{T}}} = \frac{P_{\mathrm{tot}}}{\operatorname{trace}\left(\boldsymbol{I}_M - \boldsymbol{S}_{\mathrm{TT}}^H\boldsymbol{S}_{\mathrm{TT}}\right)}\boldsymbol{I}_M$ [75, Ch. 8]. Then, the achievable sum rate is

found as

$$R = \log_2 \left[\det \left(\boldsymbol{I}_K + \frac{1}{N_0} \boldsymbol{S}_{\mathrm{RT}} \boldsymbol{K}_{a_{\mathrm{T}}}^{*} \boldsymbol{S}_{\mathrm{RT}}^{H} \right) \right]. \tag{4.5}$$

Note that, by setting the constraint on the total radiated power (P_{tot} being constant), the values of the diagonal terms of $\boldsymbol{K}_{a_{\mathrm{T}}}^{*}$ reflect the overall power losses at the ports of a BSA due to the MC between them, as it can be observed in the definition of $\boldsymbol{K}_{a_{\mathrm{T}}}^{*}$. Such analyses which only partly model the effect of MC have been traditionally performed within the signal processing community [73].

However, MC affects the total radiated power through the embedded element efficiency [76, Ch. 3.3.3], as the ability of a port to radiate the energy into space diminishes with increased coupling levels to other ports, which depends on its relative position within an antenna array. Therefore, a more practical sum rate definition involves the accepted power $\boldsymbol{P}_{\mathrm{acc}} \in \mathbb{C}^{M \times M}$ as

$$R = \log_2 \left[\det \left(\boldsymbol{I}_K + \frac{1}{N_0} \boldsymbol{S}_{\mathrm{RT}} \boldsymbol{P}_{\mathrm{acc}} \boldsymbol{S}_{\mathrm{RT}}^{H} \right) \right], \tag{4.6}$$

where

$$\boldsymbol{P}_{\mathrm{acc}} = \boldsymbol{K}_{a_{\mathrm{T}}} (\boldsymbol{I}_M - \boldsymbol{S}_{\mathrm{TT}}^{H} \boldsymbol{S}_{\mathrm{TT}}). \tag{4.7}$$

To illustrate the applicability of the model discussed in Ch. 3 to the sum-rate analysis of downlink LoS systems, the example of the system studied in Paper B is revisited. In this example, a BSA consisting of $M = 4$ center-fed half-wavelength z-oriented strip dipoles in the uniform linear array (ULA) configuration placed along the x-axis, serves $K = 2$ co-polarized single-antenna UEs. Perfect matching is assumed at both the BSA and the UEs. Moreover, the UEs are assumed as mutually uncoupled. The UEs are uniformly distributed in the H-plane far field of the BSA, within its field-of-view (FoV) chosen from $\phi = 30^\circ$ to $\phi = 150^\circ$ with 1° angular sampling. The inter-element spacings of the ULAs are varied from $d = 0.5\lambda$ to $d = 2\lambda$. For each spacing, $\boldsymbol{S}_{\mathrm{TT}}$ and the far-field EEPs of all elements of the BSA, which are used to model the channel matrix $\boldsymbol{H}$, are extracted by using the methodology described in Ch. 3. The elements of the BSA are excited by using the Thévenin voltage sources with $V_{\mathrm{T}} = 1\,\mathrm{V}$ and $Z_0 = 85\,\Omega$.

Then, the 5% outage sum rate is computed as follows. First, by considering the radiated power constraint, the sum rate is computed using (4.5) for all possible combinations of user locations in the FoV of the transmit antenna ($\phi_{k=1}, \phi_{k=2}$). Then, the worst 5% sum-rate values are discarded from the data pool. From the remaining set, the maximum (R_{max}), the average (R_{avg}) and the minimum (R_{min}) sum rates are determined and plotted in Fig. 4.3. The sum rates obtained by using the MoM-based input data computed by FEKO, are taken as the reference. For comparison, the sum rates acknowledging (superscript "MC") or ignoring (superscript "nMC") the effects of MC, are plotted in the same figure.

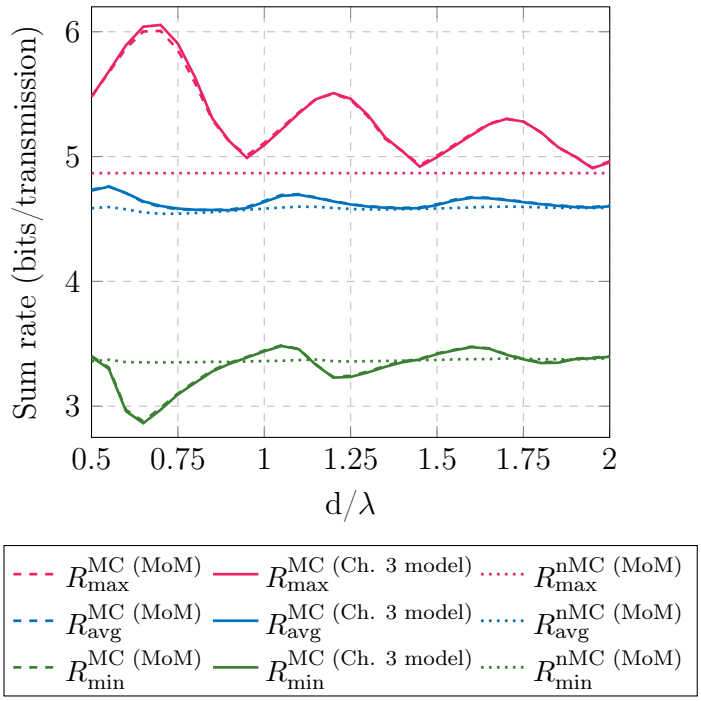

Figure 4.3: Sum rates $R_{\max}$, R_{avg} and $R_{\min}$ considering mutual coupling (MC) or assuming no mutual coupling (nMC) between the elements at the BSA.

The plots in Fig. 4.3 show good agreement between the sum rates based on the model described in Ch. 3 and the sum rates based on the reference data by FEKO for all considered inter-element spacings. As expected, with increasing inter-element separation, the curves including MC seem to converge to the "nMC" model. Moreover, the sizeable differences between the "MC" and "nMC" plots indicate the non-negligible effect of MC on the sum rate of LoS MU-MIMO systems. Additionally, the "MC" plots seem to exhibit the periodicity in the order of $\lambda/2$, which reflects the physical nature of the mutual impedance. Finally, though the practical relevance of the studied example may be limited in the context of Massive MIMO applications, the accuracy of the numerical example in Fig. 4.3, complemented with the computational rewards of the MC model observed in Paper A, make this combined approach a promising candidate-model for the efficient analysis of the sum-rate performance of Massive MU-MIMO systems.

Chapter 5

Contributions and Future Work

In the first two introductory chapters, the impact of MC on Massive MIMO systems has been reviewed, and an overview of the common strategies for the analysis of MC has been given. In addition, the potential use of sparse antenna arrays for Massive MIMO communications has been discussed. In Ch. 3, the model for the efficient analysis of sparse antenna arrays has been developed. In Ch. 4, the model for the sum-rate analysis of downlink LoS MU-MIMO systems in the presence of MC effects, extracted by using the model developed in Ch. 3, has been discussed. In this chapter, the contributions of the appended papers in Part II are summarized and placed in the context of the research goals listed in Sec. 1.4. A brief discussion regarding the possible future work directions concludes the chapter.

5.1 Contributions

5.1.1 Paper A: Fast Characterization of Mutually-Coupled Array Antennas Using Isolated Antenna Far-Field Data

This paper introduces a novel computationally-efficient strategy for the analysis of antenna array MC, which is based on the characteristics of an isolated element and relates to iterative Jacobi and Gauss-Seidel based techniques. The proposed method uses sampled far-field data of an isolated element, including the radiated far-field pattern due to excitation at the antenna port and a set of scattered far fields for several directions of incident plane waves. These data can be straightforwardly obtained using any available EM field solver and need to be computed only once. Mutual relations between the elements are modeled by approximating the incident SWE-based field scattered from other array elements as a single plane wave with mutually orthogonal polarization. Due to this far-field feature, the proposed method is primarily intended for the fast analysis of sparse antenna array configurations although, in

principle, it can be used to analyze the MC in arbitrary antenna arrays with some arbitrary element. The numerical performance of the method has been analyzed and compared to that of the MoM-based solver FEKO, showing good accuracy and significant run-time rewards in all studied numerical examples involving the sparse antenna arrays of various sizes and shapes. The performed analysis suggests a variety of potential applications of the method in the context of antenna arrays for Massive MIMO applications, ranging from the systematic analysis of MC to optimization and synthesis.

5.1.2 Paper B: Effect of Antenna Array Element Separation on Capacity of MIMO Systems Including Mutual Coupling

This paper presents the study of the effect of BSA array inter-element separation on the achievable sum rate of downlink LoS MU-MIMO systems in the presence of antenna mutual coupling. First, a two-port network model of a LoS MU-MIMO system is given. In a LoS environment, the direct-wave component from the BSA dominates the channel. Hence, the entries of the channel matrix $\boldsymbol{H}$ can be approximated with the EEPs of the transmit array. Then, the sum rate is evaluated by using the radiated power constraint capacity model, with the MC taken into account through the S-matrix of the transmit array and the channel matrix. Then, the outage performance of the downlink MU-MIMO system with 4 BS antennas and 2 single-antenna users which are uniformly distributed in the FoV of the BSA, is analyzed. The analysis demonstrates the non-negligible effect of MC on the achievable sum rates. In terms of the outage sum rate, MC seems to benefit the throughput for certain inter-element spacings, as hypothesized in Sec. 2.1.

5.2 Future Work

The main focus of this research has been dedicated towards the development of a computationally-efficient model for the analysis of sparse-array MC which is studied in Paper A. However, this model could be further improved by using the near-field data and modeling the contribution of the radial field component, in order to improve its applicability for arrays with closer inter-element spacings. Similarly, the development of a hybrid method combining a more accurate technique for the modeling of nearest-neighbor interactions, and the "SW-PW" approach described in Ch. 3 for the modeling of "far" interactions, represents another possibility. Additionally, the convergence of the iterative scheme could be possibly significantly improved by introducing the physics-based characteristic basis function patterns (CBFPs) [77] into the scheme, in what would be inspired by a similar concept applied to the iterative Jacobi-based surface currents modeling in [68].

Moreover, the successful integration of the MC model presented in Ch. 3 with the sum-rate model of a downlink LoS MU-MIMO system, as described in Ch. 4, allows for studying the impact of different array configurations in terms of the element selection and the array size and shape on the sum rate performance of Massive MIMO systems. Additionally, this model could be generalized for the NLoS scenario by applying the concepts discussed in [9, Ch. 4]. Alternatively, the run-time benefits of the MC model discussed in Ch. 3 could be exploited by integrating it into an existing synthesis scheme for sparse antenna arrays for Massive MIMO applications.

Finally, the ongoing research involves the development of iterative strategies for the efficient solution of MoM-based systems involving the finite antenna arrays. Such approach deviates from the model discussed in Ch. 3, as it treats the MC at the level of the surface currents, rather than at the level of the scattered fields. This research line presents the opportunity for the comparative convergence analysis between comparable surface-current and electric-field-based iterative schemes, which would provide deeper understanding of the convergence behavior of the modeling technique presented in Ch. 3, particularly in the context of common convergence-related linear-algebraic variables (e.g., the spectral radius of the iteration matrix or the condition number of the array impedance matrix).

References

[1] R. Ling, "Mobile communication," in *International Encyclopedia of the Social and Behavioral Sciences*, 2nd ed., J. D. Wright, Ed. Amsterdam and Oxford, UK: Elsevier, 2015, pp. 629 – 635.

[2] "Cisco Annual Internet Report (2018–2023)," White Paper, Cisco, Mar. 2020.

[3] J. Orlosky, K. Kiyokawa, and H. Takemura, "Virtual and augmented reality on the 5G highway," *J. Inf. Process.*, vol. 25, pp. 133–141, Feb. 2017.

[4] "Understanding 5G: Perspectives on future technological advancements in mobile," Analysis, GSMA Intelligence, Dec. 2014.

[5] "The Tactile Internet," Technology Watch Report, ITU-T, Aug. 2014.

[6] T. L. Marzetta, "Massive MIMO: An introduction," *Bell Labs Technical J.*, vol. 20, pp. 11–22, Mar. 2015.

[7] European Commission. (2016, Sep.) 5G for Europe: An action plan. [Online]. Available: https://ec.europa.eu/digital-single-market/en/news/communication-5g-europe-action-plan-and-accompanying-staff-working-document

[8] L. Sanguinetti, E. Björnson, and J. Hoydis, "Toward Massive MIMO 2.0: Understanding spatial correlation, interference suppression, and pilot contamination," *IEEE Trans. Commun.*, vol. 68, no. 1, pp. 232–257, Jan. 2020.

[9] N. Amani, "Sparse array architectures for 5G base station antenna design," Licentiate thesis, Chalmers University of Technology, Göteborg, May 2019. [Online]. Available: https://chalmersuniversity.app.box.com/s/iofp9jysixo0lrr89brlecf14j74lik8

[10] T. L. Marzetta, E. G. Larsson, H. Yang, and H. Q. Ngo, *Fundamentals of Massive MIMO*. Cambridge, UK: Cambridge University Press, 2016.

References

[11] E. Björnson, J. Hoydis, and L. Sanguinetti, "Massive MIMO networks: Spectral, energy, and hardware efficiency," *Foundations and Trends® in Signal Process.*, vol. 11, no. 3-4, pp. 154–655, Nov. 2017.

[12] J. H. Winters, "Optimum combining in digital mobile radio with cochannel interference," *IEEE J. Sel. Areas Commun.*, vol. SAC-2, no. 4, pp. 528–539, Jul. 1984.

[13] S. C. Swales, M. A. Beach, D. J. Edwards, and J. P. McGeehan, "The performance enhancement of multibeam adaptive base-station antennas for cellular land mobile radio systems," *IEEE Trans. Veh. Technol.*, vol. 39, no. 1, pp. 56–67, Feb. 1990.

[14] S. Anderson, M. Millnert, M. Viberg, and B. Wahlberg, "An adaptive array for mobile communication systems," *IEEE Trans. Veh. Technol.*, vol. 40, no. 1, pp. 230–236, Feb. 1991.

[15] E. Björnson, L. Sanguinetti, H. Wymeersch, J. Hoydis, and T. L. Marzetta, "Massive MIMO is a reality—What is next? Five promising research directions for antenna arrays," *Digit. Signal Process.*, vol. 94, pp. 3 – 20, Nov. 2019, special Issue on Source Localization in Massive MIMO.

[16] T. L. Marzetta, "Noncooperative cellular wireless with unlimited numbers of base station antennas," *IEEE Trans. Wireless Commun.*, vol. 9, no. 11, pp. 3590–3600, Nov. 2010.

[17] H. Q. Ngo, E. G. Larsson, and T. L. Marzetta, "Aspects of favorable propagation in Massive MIMO," in *2014 22nd European Signal Process. Conf. (EUSIPCO)*, Lisbon, Portugal, Sep. 2014, pp. 76–80.

[18] E. Björnson. (2017, Oct.) Six differences between Massive MIMO and MU-MIMO. [Online]. Available: http://ma-mimo.ellintech.se/2017/10/17/six-differences-between-mu-mimo-and-massive-mimo

[19] H. Yang and T. L. Marzetta, "Performance of conjugate and zero-forcing beamforming in large-scale antenna systems," *IEEE J. Sel. Areas Commun.*, vol. 31, no. 2, pp. 172–179, Feb. 2013.

[20] E. G. Larsson, O. Edfors, F. Tufvesson, and T. L. Marzetta, "Massive MIMO for next generation wireless systems," *IEEE Commun. Mag.*, vol. 52, no. 2, pp. 186–195, Feb. 2014.

[21] J. Hoydis, S. ten Brink, and M. Debbah, "Massive MIMO in the UL/DL of cellular networks: How many antennas do we need?" *IEEE J. Sel. Areas Commun.*, vol. 31, no. 2, pp. 160–171, Feb. 2013.

[22] A. Fehske, J. Malmodin, G. Biczók, and G. Fettweis, "The global carbon footprint of mobile communications: The ecological and economic perspective," *IEEE Commun. Mag.*, vol. 49, pp. 55–62, Aug. 2011.

[23] A. Di Ciaula, "Towards 5G communication systems: Are there health implications?" *Int. J. Hyg. Environ. Health*, vol. 221, no. 3, pp. 367 – 375, Apr. 2018.

[24] K. R. Foster, S. Kodera, and A. Hirata, "5G communications systems and radiofrequency exposure limits," *IEEE Future Netw. Tech Focus*, vol. 3, no. 2, Sep. 2019.

[25] F. Pereira de Figueiredo, F. Cardoso, I. Moerman, and G. Fraidenraich, "Channel estimation for Massive MIMO TDD systems assuming pilot contamination and frequency selective fading," *IEEE Access*, vol. 5, pp. 17 733–17 741, Sep. 2017.

[26] C. Craeye and D. González-Ovejero, "A review on array mutual coupling analysis," *Radio Sci.*, vol. 46, RS2012, no. 2, pp. 1–25, Apr. 2011.

[27] H. Q. Ngo, A. Ashikhmin, H. Yang, E. G. Larsson, and T. L. Marzetta, "Cell-free massive MIMO versus small cells," *IEEE Trans. Wireless Commun.*, vol. 16, no. 3, pp. 1834–1850, Mar. 2017.

[28] E. Björnson, L. Van der Perre, S. Buzzi, and E. G. Larsson, "Massive MIMO in sub-6 GHz and mmWave: Physical, practical, and use-case differences," *IEEE Wireless Commun.*, vol. 26, no. 2, pp. 100–108, Apr. 2019.

[29] G. Toso, C. Mangenot, and A. G. Roederer, "Sparse and thinned arrays for multiple beam satellite applications," in *2nd European Conf. Antennas Propag., EuCAP 2007*, Edinburgh, UK, Nov. 2007, pp. 1–4.

[30] C. Bencivenni, "Sparse array synthesis of complex antenna elements," Licentiate thesis, Chalmers University of Technology, Göteborg, Jun. 2015. [Online]. Available: http://publications.lib.chalmers.se/records/fulltext/217000/217000.pdf

[31] J. G. Bij de Vaate, D. B. Davidson, and S. J. Wijnholds, "Regular sparse arrays: The impact of grating lobes on radio astronomical observations," in *2nd URSI Atlantic Radio Sci. Meeting (AT-RASC 2018)*, Gran Canaria, Spain, May 2018, pp. 1–3.

[32] W. A. van Cappellen, S. J. Wijnholds, and J. D. Bregman, "Sparse antenna array configurations in large aperture synthesis radio telescopes," in *Proc. 3rd European Radar Conf. (EURAD 2006)*, Manchester, UK, Sep. 2006, pp. 76–79.

References

[33] B. Klopper, "Antenna elements for sparse-regular aperture arrays," Ph.D. dissertation, Stellenbosch University, Stellenbosch, Apr. 2019. [Online]. Available: https://scholar.sun.ac.za/handle/10019.1/105722

[34] T. Marinovic, D. I. L. de Villiers, D. Bekers, M. N. Johansson, A. Stjernman, R. Maaskant, and G. A. E. Vandenbosch, "Fast characterization of mutually-coupled array antennas using isolated antenna far-field data," *IEEE Trans. Antennas Propag.*, vol. 68, 2020, in press.

[35] P.-S. Kildal, *Foundations of Antenna Engineering: A Unified Approach for Line-of-Sight and Multipath.* Gothenburg: Kildal Antenn AB, Apr. 2015.

[36] C.-M. Chen, V. Volski, L. Van der Perre, G. A. E. Vandenbosch, and S. Pollin, "Finite large antenna arrays for Massive MIMO: Characterization and system impact," *IEEE Trans. Antennas Propag.*, vol. 65, no. 12, pp. 6712–6720, Dec. 2017.

[37] P.-S. Kildal and K. Rosengren, "Correlation and capacity of MIMO systems and mutual coupling, radiation efficiency, and diversity gain of their antennas: Simulations and measurements in a reverberation chamber," *IEEE Commun. Mag.*, vol. 42, no. 12, pp. 104–112, Dec. 2004.

[38] W. Kahn, "Active reflection coefficient and element efficiency in arbitrary antenna arrays," *IEEE Trans. Antennas Propag.*, vol. 17, no. 5, pp. 653–654, Sep. 1969.

[39] Y. Gao, R. Ma, Y. Wang, Q. Zhang, and C. Parini, "Stacked patch antenna with dual-polarization and low mutual coupling for Massive MIMO," *IEEE Trans. Antennas Propag.*, vol. 64, no. 10, pp. 4544–4549, Oct. 2016.

[40] H. Huang, X. Li, and Y. Liu, "A low-profile, dual-polarized patch antenna for 5G MIMO application," *IEEE Trans. Antennas Propag.*, vol. 67, no. 2, pp. 1275–1279, Feb. 2019.

[41] X. Chen, S. Zhang, and Q. Li, "A review of mutual coupling in MIMO systems," *IEEE Access*, vol. 6, pp. 24 706–24 719, Apr. 2018.

[42] A. Jafargholi, A. Jafargholi, and J. H. Choi, "Mutual coupling reduction in an array of patch antennas using CLL metamaterial superstrate for MIMO applications," *IEEE Trans. Antennas Propag.*, vol. 67, no. 1, pp. 179–189, Jan. 2019.

[43] P.-S. Kildal and K. Rosengren, "Electromagnetic analysis of effective and apparent diversity gain of two parallel dipoles," *IEEE Antennas Wireless Propag. Lett.*, vol. 2, pp. 9–13, 2003.

[44] R. L. Haupt, *Antenna Arrays: A Computational Approach.* Hoboken, NJ: John Wiley and Sons. Inc., 2010.

[45] A. H. Mohammadian, S. S. Soliman, M. A. Tassoudji, and L. Golovanevsky, "A closed-form method for predicting mutual coupling between base-station dipole arrays," *IEEE Trans. Veh. Technol.*, vol. 56, no. 3, pp. 1088–1099, May 2007.

[46] M. E. Bialkowski, P. Uthansakul, K. Bialkowski, and S. Durrani, "Investigating the performance of MIMO systems from an electromagnetic perspective," *IEEE Microw. Opt. Technol. Lett.*, vol. 48, no. 7, pp. 1233 – 1238, Jul. 2006.

[47] P. Meerasri, P. Uthansakul, and M. Uthansakul, "Self-interference cancellation-based mutual-coupling model for full-duplex single-channel MIMO systems," *Int. J. Antennas Propag.*, vol. 2014, pp. 1–10, Jan. 2014.

[48] F. Gustrau and D. Manteuffel, *EM Modeling of Antennas and RF Components for Wireless Communication Systems.* Berlin and Heidelberg: Springer-Verlag, 2006.

[49] J. Song, C.-C. Lu, and W. C. Chew, "Multilevel fast multipole algorithm for electromagnetic scattering by large complex objects," *IEEE Trans. Antennas Propag.*, vol. 45, no. 10, pp. 1488–1493, Oct. 1997.

[50] Ö. Ergül and L. Gürel, *The Multilevel Fast Multipole Algorithm (MLFMA) for Solving Large-Scale Computational Electromagnetics Problems*, ser. IEEE Press Series on Electromagnetic Wave Theory, A. C. Cangellaris, Ed. Piscataway, NJ, USA: John Wiley and Sons, Ltd, 2014.

[51] D. Ludick, U. Jakobus, and D. B. Davidson, "Efficient analysis of finite antenna arrays using the domain Green's function method," in *Proc. 2012 IEEE Int. Symp. Antennas Propag.*, Chicago, IL, Jul. 2012, pp. 1–2.

[52] E. Suter and J. Mosig, "A subdomain multilevel approach for the efficient MoM analysis of large planar antennas," *IEEE Microw. Opt. Technol. Lett.*, vol. 26, no. 4, pp. 270 – 277, Aug. 2000.

[53] E. Lucente, G. Tiberi, A. Monorchio, G. Manara, and R. Mittra, "The characteristic basis function method (CBFM): A numerically efficient strategy for solving large electromagnetic scattering problems," *Turkish J. Electr. Eng.*, vol. 16, no. 1, pp. 41–56, 2008.

[54] R. Maaskant, R. Mittra, and A. Tijhuis, "Fast analysis of large antenna arrays using the characteristic basis function method and the adaptive cross approximation algorithm," *IEEE Trans. Antennas Propag.*, vol. 56, no. 11, pp. 3440–3451, Nov. 2008.

References

[55] L. Matekovits, V. A. Laza, and G. Vecchi, "Analysis of large complex structures with the synthetic-functions approach," *IEEE Trans. Antennas Propag.*, vol. 55, no. 9, pp. 2509–2521, Sep. 2007.

[56] Kezhong Zhao, M. N. Vouvakis, and Jin-Fa Lee, "The adaptive cross approximation algorithm for accelerated method of moments computations of EMC problems," *IEEE Trans. Electromagn. Compat.*, vol. 47, no. 4, pp. 763–773, Nov. 2005.

[57] Altair. (2019, Mar.) FEKO MLFMM. [Online]. Available: https://blog.altair.co.kr/wp-content/uploads/2019/03/Webinar_MLFMM.pdf

[58] D. Ludick, R. Maaskant, D. B. Davidson, U. Jakobus, and R. Mittra. (2014, May) A comparison of domain decomposition techniques for analysing disjoint finite antenna arrays. [Online]. Available: https://www.e-fermat.org/files/multimedias/1536a903215cc4.pdf

[59] M. I. Mishchenko, L. D. Travis, and D. W. Mackowski, "T-matrix method and its applications to electromagnetic scattering by particles: A current perspective," *J. Quantitative Spectroscopy Radiative Transfer*, vol. 111, no. 11, pp. 1700–1703, 2010.

[60] M. Fruhnert, I. Fernandez-Corbaton, V. Yannopapas, and C. Rockstuhl, "Computing the T-matrix of a scattering object with multiple plane wave illuminations," *Beilstein J. Nanotechnol.*, vol. 8, pp. 614–626, Mar. 2017.

[61] J. Rubio, M. A. González, and J. Zapata, "Generalized-scattering-matrix analysis of a class of finite arrays of coupled antennas by using 3-D FEM and spherical mode expansion," *IEEE Trans. Antennas Propag.*, vol. 53, no. 3, pp. 1133–1144, Mar. 2005.

[62] F. J. Demuynck, G. A. E. Vandenbosch, and A. R. Van de Capelle, "The expansion wave concept—Part I: Efficient calculation of spatial Green's functions in a stratified dielectric medium," *IEEE Trans. Antennas Propag.*, vol. 46, no. 3, pp. 397–406, Mar. 1998.

[63] G. A. E. Vandenbosch and F. J. Demuynck, "The expansion wave concept—Part II: A new way to model mutual coupling in microstrip arrays," *IEEE Trans. Antennas Propag.*, vol. 46, no. 3, pp. 407–413, Mar. 1998.

[64] S. Lou, B. Duan, W. Wang, C. Ge, and S. Qian, "Analysis of finite antenna arrays using the characteristic modes of isolated radiating elements," *IEEE Trans. Antennas Propag.*, vol. 67, no. 3, pp. 1582–1589, Mar. 2019.

[65] Y. Liu, A. Ren, H. Liu, H. Wang, and C. Sim, "Eight-port MIMO array using characteristic mode theory for 5G smartphone applications," *IEEE Access*, vol. 7, pp. 45 679–45 692, Apr. 2019.

[66] C. Bencivenni, M. V. Ivashina, R. Maaskant, and J. Wettergren, "Synthesis of maximally sparse arrays using compressive sensing and full-wave analysis for global Earth coverage applications," *IEEE Trans. Antennas Propag.*, vol. 64, no. 11, pp. 4872–4877, Nov. 2016.

[67] ——, "Design of maximally sparse antenna arrays in the presence of mutual coupling," *IEEE Antennas Wireless Propag. Lett.*, vol. 14, pp. 159–162, 2015.

[68] D. J. Ludick, M. M. Botha, R. Maaskant, and D. B. Davidson, "The CBFM-enhanced Jacobi method for efficient finite antenna array analysis," *IEEE Antennas Wireless Propag. Lett.*, vol. 16, pp. 2700–2703, 2017.

[69] D. I. L. de Villiers and R. Maaskant, "Element pattern prediction in mutually-coupled arrays through isolated antenna characterization," in *2017 Int. Symp. Antennas Propag. (ISAP)*, Phuket, Thailand, Oct. 2017, pp. 1–2.

[70] K. Pontoppidan, "GRASP technical description," TICRA, Copenhagen, Denmark, Tech. Rep. 10.5.0, Jun. 2015.

[71] T. Marinović, A. Farsaei, R. Maaskant, A. Lahuerta-Lavieja, M. N. Johansson, U. Gustavsson, and G. A. E. Vandenbosch, "Effect of antenna array element separation on capacity of MIMO systems including mutual coupling," in *IEEE Int. Symp. Antennas Propag. and USNC-URSI Radio Sci. Meeting*, Atlanta, GA, USA, Jul. 2019, pp. 415–416.

[72] J. A. Dobrowolski, *Introduction to Computer Methods for Microwave Circuit Analysis and Design.* Warsaw University of Technology: Artech House, 1991.

[73] J. W. Wallace and M. A. Jensen, "The capacity of MIMO wireless systems with mutual coupling," in *Proc. IEEE 56th Veh. Technol. Conf. (VTC 2002)*, Vancouver, BC, Canada, Sep. 2002, pp. 696–700.

[74] ——, "Mutual coupling in MIMO wireless systems: A rigorous network theory analysis," *IEEE Trans. Wireless Commun.*, vol. 3, no. 4, pp. 1317–1325, Jul. 2004.

[75] D. Tse and P. Viswanath, *Fundamentals of Wireless Communication.* New York, NY, USA: Cambridge University Press, 2005.

References

[76] P.-S. Kildal, M. Franzen, M. V. Ivashina, and W. van Cappellen, "Measurement of embedded element efficiencies of wideband dense arrays in reverberation chamber," in *2nd European Conf. Antennas Propag., EuCAP 2007*, Edinburgh, UK, Nov. 2007, pp. 1–4.

[77] R. Maaskant, M. V. Ivashina, S. J. Wijnholds, and K. F. Warnick, "Efficient prediction of array element patterns using physics-based expansions and a single far-field measurement," *IEEE Trans. Antennas Propag.*, vol. 60, no. 8, pp. 3614–3621, Aug. 2012.